Inferring potential landslide damming using slope stability, geomorphic constraints and run-out analysis; case study from the NW Himalaya

Vipin Kumar[1*], Imlirenla Jamir[2], Vikram Gupta[3], Rajinder K. Bhasin[4]

[1]Georisks and Environment, Department of Geology, University of Liege, Liege, Belgium
[2]Public Works Department (PWD), Nagaland, India
[3]Wadia Institute of Himalayan Geology, Dehradun, India
[4]Norwegian Geotechnical Institute, Oslo, Norway

*Correspondence: v.chauhan777@gmail.com; B-18, B-4000, Sart-Tilman, Liege, Belgium

ABSTRACT

Prediction of potential landslide damming has been a difficult process owing to the uncertainties related to landslide volume, resultant dam volume, entrainment, valley configuration, river discharge, material composition, friction, and turbulence associated with material. In this study, instability pattern of landslides, geomorphic indices, post failure run-out predictions, and spatio-temporal patterns of rainfall and earthquakes are explored to predict the potential landslide damming sites. The Satluj valley, NW Himalaya is chosen as a case study area. The study area has witnessed landslide damming in the past and incurred losses of $ ~30M and 350 lives in the last four decades due to such processes. Forty-four active landslides that cover a total ~4.81 ± 0.05 x 10^6 m^2 area and ~34.1 ± 9.2 x 10^6 m^3 volume are evaluated to identify those landslides that may result in potential landslide damming. Out of forty-four, five landslides covering a total volume of ~26.3 ± 6.7 x 10^6 m^3 are noted to form the potential landslide dams. Spatio-temporal variations in the pattern of rainfall in the recent years enhanced the possibility of landslide triggering and hence of potential damming. These five landslides also revealed 24.8 ± 2.7m to 39.8± 4.0m high debris flows in the run-out predictions.

Key words: Landslide damming, Slope stability; Run-out; Himalaya

1.0 INTRODUCTION

Landslide damming is a normal geomorphic process in narrow river valleys and poses significant natural hazard (Dai et al. 2005; Gupta and Sah 2008; Delaney and Evans 2015; Fan et al. 2020). Many studies have explored damming characteristics (Li et al. 1986; Costa and Schuster 1988; Takahashi and Nakawaga 1993; Ermini and Casagli 2003; Fujisawa et al. 2009; Stefanelli et al. 2016; Kumar et al. 2019a). However, studies concerning the prediction of potential landslide dams and their stability at regional scale have been relatively rare, particularly in Himalaya despite a history of landslide damming and flash floods (Gupta and Sah 2008; Ruiz-Villanueva et al. 2016; Kumar et al. 2019a). In order to identify the landslides that have potential to form dams, the following factors have been main requisites; (i) pre- and post-failure behaviour of landslide slopes, and (ii) landslide volume, stream power, and morphological setting of the valley (Kumar et al. 2019a).

To understand the pre-failure pattern, Finite Element Method (FEM) based slope stability evaluation has been among the most widely used approaches for complex slope geometry (Griffiths and Lane 1999; Jing 2003; Jamir et al. 2017; Kumar et al. 2018). However, the selection of input parameters in FEM analysis and the set of assumptions used (material model, failure criteria, and convergence) may also result in uncertainty in the final output (Wong 1984; Cho 2007; Li et al. 2016). Uncertainty from input parameters can be resolved by performing parametric analysis, whereas the utilization of most appropriate criteria can minimize the uncertainty caused by assumptions. Post-failure behavior of landslides can be understood using run-out analysis (Hungr et al. 1984; Hutter et al. 1994; Rickenmann and Scheidl 2013). These methods could be classified into empirical/statistical and dynamical categories (Rickenmann 2005). Owing to the flexibility in rheology, solution approach, reference frame, and entrainment, dynamic models have been relatively more realistic for site-specific problems (Corominas and Mavrouli 2011). Though the different numerical models have different advantages and limitations, Voellmy rheology (friction and turbulence) (Voellmy 1955; Salm 1993) based Rapid Mass Movement Simulation (RAMMS) (Christen et al. 2010) has been used widely owing to the inclusion of rheological and entrainment rate flexibility.

Apart from the pre and post-failure pattern, landslide volume, stream power and morphological setting of the valley are crucial to infer the potential landslide damming. The Morphological Obstruction Index (MOI) and Hydro-morphological Dam Stability Index (HDSI) have been

widely used geomorphic indices to infer the potential of landslide dam formation and their temporal stability (Costa and Schuster 1988; Ermini and Casagli 2003; Stefanelli et al. 2016).

The NW Himalaya has been one of most affected terrains by the landslides owing to the active tectonics and multiple precipitation sources i.e., Indian Summer Monsoon (ISM) and Western Disturbance (Dimri et al. 2015). The NW Himalaya has accommodated ~51 % of all the landslides in India during yrs. 1800-2011 (Parkash 2011). The Satluj River valley, NW Himalaya is one such region where landslides and associated floods have claimed ~350 lives and resulted in the loss of minimum 30 million USD in the last four decades. This region holds a high potential for future landslide damming and resultant floods (Ruiz-Villanueva et al. 2016; Kumar et al. 2019a). Therefore, the Satluj valley is taken as a case study area, and 44 active landslides belonging to the different litho-tectonic regimes are modeled using the FEM technique. Multiple slope sections and a range of values of different input parameters are used to perform the parametric study. In order to determine the human population that might be affected by these landslides, census statistics are also used. The MOI and HDSI are used to determine the potential of landslide dam formation and their stability, respectively. In view of the role of rainfall and earthquakes as main landslide triggering factors, the spatio-temporal regime of these two factors is also discussed. Run-out prediction of certain landslides is also performed to understand the role of run-out in the potential landslide damming. This study provides detailed insight into the regional instability pattern, associated uncertainty, and potential landslide damming sites and hence it can be replicated in other hilly terrain witnessing frequent landslides and damming.

2.0 STUDY AREA

The study area is located between the Moorang (31˚36′1″ N, 78˚26′ 47″ E) and Rampur town (31˚27′10″ N, 77˚38′ 20″ E) in the Satluj River valley, NW Himalaya (Fig. 1). The Satluj River flows across the Tethyan Sequence (TS), Higher Himalaya Crystalline (HHC), Lesser Himalaya Crystalline (LHC), and Lesser Himalaya Sequence (LHS). The TS in the study area comprises slate/phyllite and schist and has been intruded by the biotite-rich granite i.e., Kinnaur-Kailash Granite (KKG) near the Sangla Detachment (SD) fault (Sharma 1977; Vannay et al. 2004). The SD fault separates the TS from the underlying crystalline rockmass of the HHC. Migmatitic gneiss marks the upper part of the HHC, whereas the base is marked by the kyanite-sillimanite gneiss rockmass (Sharma 1977; Vannay et al. 2004; Kumar et al. 2019b). The Main Central Thrust (MCT) fault separates the HHC from the underlying schist/gneissic

rockmass of the LHC. The LHC comprises mica schist, carbonaceous schist, quartzite, and amphibolite. A thick zone of gneiss i.e., Wangtu Gneissic Complex (WGC) is exposed in the LHC, which comprises augen gneiss and porphyritic granitoids. The LHC is delimited at the base by the Munsiari Thrust (MT) fault that is thrusted over the Lesser Himalaya Sequence (LHS) rockmass. The MT contains breccia, cataclastic, and fault gouge (Sharma 1977; Vannay et al. 2004; Kumar et al. 2019b). The LHS in the study area consists of quartz-arenite (Rampur Quartzite) with bands of phyllite, meta-volcanics, and paragneiss (Sharma 1977).

The present study covers forty-four active landslides (20 debris slides, 13 rock falls, and 11 rock avalanches) along the study area (Table 1) that have been mapped recently by Kumar et al. (2019b). Field photographs of some of these landslides are presented in Fig. 2. The TS and LHS in the study area have been subjected to relative tectonic tranquility with exhumation rates as low as 0.5 - 1.0 mm/yr, whereas the HHC and LHC region have undergone 1.0 - 4.5 mm/yr rate of exhumation (Thiede et al. 2009). The MCT fault region and the WGC are noted to have maximum exhumation rate (i.e., ~4.5 mm/yr) that is evident from the deep gorges in these regions (Fig. 2c, 2e). A majority of the earthquake events in the study area in the last 7 decades have been related to the N-S oriented Kaurik - Chango Fault (KCF) (Kundu et al. 2014; Hazarika et al. 2017; International Seismological Centre Catalogue 2019). The climate in the study area shows a spatial variation from humid (~800 mm/yr mean annual precipitation) in the LHS to the semi-arid (~200 mm/yr) in the TS (Kumar et al. 2019b). The HHC acts as a transition zone where climate varies from semi-humid to semi-arid in the SW-NE direction. This transition has been attributed to the 'orographic barrier' nature of the HHC that marks the region in its north as 'orographic interior' and the region to its south as the 'orographic front' (Wulf et al. 2012; Kumar et al. 2019b).

Landslides in the study area have been a consistent threat to the socio-economic condition of the nearby human population (Gupta and Sah 2008; Ruiz-Villanueva et al. 2016; Kumar et al. 2019a). Therefore, the human population in the vicinity of each landslide was also determined by considering the nearby villages/town. Notably, a total of 25,822 people reside within 500 m extent of the 44 landslide slopes, and about 70 % of this population is residing in the reach of debris slide type landslides. Since the Govt. of India follows a 10 year gap in census statistics, the human population data was based on last official data i.e., Census-2011. The next official census is due in year 2021. The population density in the Indian Himalayan region was estimated to be 181/km² in the year 2011 that might grow to 212/km² in 2021 with a decadal

growth rate of 17.3% (https://censusindia.gov.in, retrieved on 02 Sep 2020; http://gbpihedenvis.nic.in, retrieved on 02 Sep 2020).

3.0 METHODOLOGY

The methodology involved field data collection, satellite imagery analysis, laboratory analyses, slope stability modelling, geomorphic indices, rainfall/earthquake pattern and run-out modelling. Details are as follows;

3.1 Field data, satellite imagery processing, and laboratory analyses

The field work involved rock/soil sample collection from each landslide location, rockmass joint mapping, and N-type Schmidt Hammer Rebound (SHR) measurement. Joints were included in the slope models for the FEM based slope stability analysis. The dataset involving the joint details is available in the data repository (Kumar et al. 2021). The SHR values were obtained as per International Society of Rock Mechanics (ISRM) standard (Aydin 2008). Cartosat-1 satellite imagery and field assessment were used to finalize the location of slope sections (2D) of the landslides. Cartosat-1 imagery has been used widely for the landslide related studies (Martha et al. 2010). The Cartosat-1 Digital Elevation Model (DEM) having 10m spatial resolution, prepared using the Cartosat-1 stereo imagery, was used to extract the slope sections of the landslides using the Arc GIS-10.2 software. Details of the satellite imagery are mentioned in Table 2.

The rock/soil samples were analyzed in the National Geotechnical Facility (NGF) and Wadia Institute of Himalayan Geology (WIHG) laboratory, India. The rock samples were drilled and smoothed for Unconfined Compressive Strength (UCS) (IS: 9143-1979) and ultrasonic tests (CATS Ultrasonic (1.95) of Geotechnical Consulting & Testing Systems). The ultrasonic test was conducted to determine the density, elastic modulus, and Poisson's ratio of rock samples. The soil samples were tested for grain size (IS: 2720-Part 4-1985), UCS test (IS: 2720-Part 10-1991), and direct shear test (IS: 2720-Part 13- 1986). If the soil samples contained < 5% fines (< 75 mm), the hydrometer test was not performed for the remaining fine material. In the direct shear test, soil samples were sheared under the constant normal stress of 50, 100 and 150 kN/m^2. The UCS test of soil was performed under three different rates of movements i.e., 1.25 mm/min, 1.50 mm/min and 2.5 mm/min.

3. 2 Slope stability modelling

142 The Finite Element Method (FEM) was used along with the Shear Strength Reduction (SSR)
143 technique to infer the critical Strength Reduction Factor (SRF), Shear Strain (SS), and Total
144 Displacement (TD) in the 44 landslide slopes using the RS2 software. The SRF has been
145 observed to be similar in nature to the Factor of Safety (FS) of the slope (Zienkiewicz et al.
146 1975; Griffiths and Lane 1999). To define the failure in the SSR approach, non-convergence
147 criteria were used (Nian et al. 2011). The boundary condition with the restraining movement
148 was applied to the base and back, whereas the front face was kept free for the movement (Fig.
149 3). In-situ field stress was adjusted in view of dominant stress i.e., extension or compression,
150 by changing the value of the coefficient of earth pressure (k). A value of $k = \sigma_h/\sigma_v = 0.5$ was
151 used in extensional regime, whereas $k = \sigma_h/\sigma_v = 1.5$ was used in compressional regime. The
152 Tethyan Sequence has been observed to possess the NW-SE directed extensional regime. The
153 structures in the upper part of the HHC are influenced by the east directed extension along the
154 SD fault. The lower part, however, is characterized by the SW directed compression along the
155 Main Central Thrust. In contrast to the HHC, structures in the Lesser Himalaya Crystalline and
156 Munsiari Thrust region are influenced by the compressional regime. In the Lesser Himalaya
157 Sequence region, the SW directed compressional regime has been observed on the basis of the
158 SW verging folds, crenulation cleavage, and other features (Vannay et al. 2004).

159 The soil and rock mass were used in the models through the Mohr-Coulomb (M-C) failure
160 criterion (Coulomb 1776; Mohr 1914) and Generalized Hoek-Brown (GHB) criterion (Hoek et
161 al. 1995), respectively. The parallel- statistical distribution of the joints with normal-distributed
162 joint spacing in the rock mass was applied through the Barton-Bandis (B-B) slip criterion
163 (Barton and Choubey 1977; Barton and Bandis 1990). Plane strain triangular elements having
164 6 nodes were used through the graded mesh in the models. Details of the criteria used in the
165 FEM analysis are mentioned in Table 3. The dataset of input parameters used in the FEM
166 analysis is available in the data repository (Kumar et al. 2021). It is to note that the FEM
167 analysis was performed under the static load i.e., field stress and body force. The dynamic
168 analysis was not performed, at present, in absence of any major seismic events in the region in
169 the last 4 decades (sec. 4.3) and lack of reliable dynamic load data of nearby major seismic
170 events.

171 To understand the uncertainty caused by the selection of 2D slope section, multiple slope
172 sections were taken, wherever possible. More than one slope section was modeled for each
173 debris slide, whereas for the rock falls/ rock avalanche only one slope section was chosen due
174 to the limited width of the rock falls/rock avalanche in the study area. To find out the relative

influence of different input parameters on the final output, a parametric study was performed. In the parametric study for debris slides, Akpa landslide (S.N.5 in Fig. 3), Pangi landslide (S.N.13 in Fig. 3), and Barauni Gad landslide (S.N.38 in Fig. 3) were chosen, whereas Tirung khad (S.N.2 in Fig.3) and Chagaon landslide (S.N.21 in Fig. 3) were considered to represent rock fall. Baren Dogri (S.N.7 in Fig. 3) landslide was used to represent the rock avalanches. The selection of these landslides for the parametric study was based on the following two factors; (1) to choose the landslides from different litho-tectonic regime, and (2) to represent varying stress regime i.e., extensional, compressional, and relatively stagnant. The Parametric study of the debris slide models involved following 9 parameters; field stress coefficient, stiffness ratio, cohesion and angle of friction of soil, elastic modulus and Poisson's ratio of soil, rockmass modulus, Poisson's ratio and uniaxial compressive strength of rock. For the rockfalls/rock avalanche, the following 6 parameters were considered; uniaxial compressive strength of rock, rockmass modulus of rock, Poisson's ratio of rock, 'm_i' parameter, stiffness ratio, and field stress coefficient. The 'm_i' is a Generalized Hoek-Brown (GHB) parameter that is equivalent to the angle of friction of Mohr-coulomb (M-C) criteria.

3. 3 Geomorphic indices

Considering the possibility of landslide dam formation in case of slope failure, the following geomorphic indices were also used;

(i) Morphological Obstruction Index (MOI)

$$MOI = \log (V_l/W_v) \quad \textbf{Eq. 1}$$

(ii) Hydro-morphological Dam Stability Index (HDSI)

$$HDSI = \log (V_d/A_b.S) \quad \textbf{Eq. 2}$$

Where, V_d (dam volume)$=$ V_l (landslide volume), m^3; A_b is upstream catchment area (km^2); W_v is width of the valley (m) and S is local slope gradient of river channel (m/m). Though the resultant dam volume could be higher or lower than the landslide volume owing to slope entrainment, rockmass fragmentation, retaining of material at the slope, and washout by the river (Hungr and Evans 2004; Dong et al. 2011), dam volume is assumed to be equal to landslide volume for the worst case. By utilizing the comprehensive dataset of ~300 landslide dams of Italy, Stefanelli et al. (2016) have classified the MOI into (i) non-formation domain:

MOI <3.00, (ii) uncertain evolution domain: 3.00 <MOI >4.60, and (iii) formation domain: MOI >4.60. By utilizing the same dataset, Stefanelli et al. (2016) defined the HDSI into following categories (i) instability domain: HDSI <5.74, (ii) uncertain determination domain: 5.74<HDSI >7.44, and (iii) Stability domain: HDSI>7.44.

3. 4 Rainfall and Earthquake regime

Precipitation in the study area is related primarily to the Indian Summer Monsoon (ISM) and Western Disturbance (WD) and varies spatially-temporally due to various local and regional factors (Gadgil et al. 2007; Hunt et al. 2018). Therefore, we have taken the TRMM_3B42 (Huffman et al. 2016) daily rainfall data of years 2000-2019 at four different locations; Moorang, Kalpa, Nachar, and Rampur (Locations mentioned in Fig. 1). The dataset of earthquake events (2<M<8) in and around study area during the years 1940-2019 was retrieved from the ISC catalogue (http://www.isc.ac.uk/iscbulletin/search/catalogue/, retrieved on 02 March 2020) to determine the spatio-temporal pattern.

3. 5 Run-out modelling

Since the study area has witnessed many disastrous landslides, mostly rainfall triggered, and flash floods in past (Gupta and Sah 2008; Ruiz-Villanueva et al. 2016), run-out analysis was performed to understand the post-failure scenario. Such run-out predictions will also be helpful to ascertain the possibility of damming because various studies have noted river damming by the debris flows (Li et al. 2011; Braun et al. 2018; Fan et al. 2020). The landslides that have potential to form dams based on the indices (sec. 3.3) are evaluated for such run-out analysis.

In this study, Voellmy rheology (Voellmy 1955; Salm 1993) based Rapid Mass Movement Simulation (RAMMS) (Christen et al. 2010) model was used to understand the run-out pattern. The RAMMS for debris flow uses the Voellmy friction law and divides the frictional resistance into a dry-Coulomb type friction (μ) and viscous-turbulent friction (ξ). The frictional resistance S (Pa) is :

$$S = \mu N + (\rho g u^2)/\xi \qquad \textbf{Eq. 3}$$

where $N = \rho h g \cos(\phi)$ is the normal stress on the running surface, ρ is density, g is gravitational acceleration, ϕ is slope angle, h is flow height and u= (ux, uy), consisting of the flow velocity in the x- and y-directions. In this study, a range of friction (μ) and turbulence (ξ) values, apart from other input parameters, are used to evaluate the uncertainty in output (Table 4). Generally,

the values for μ and ξ are determined using the reconstruction of real events through the simulation and subsequent comparison between the dimensional characteristics of real and simulated event. However, the landslides in the study area merge with the river floor and/or are in close proximity and hence there is no failed material left from the previous events to reconstruct. Therefore, the μ and ξ values were taken from a range in view of topography of landslide slope and run-out path, landslide material, similar landslide events/material, and results from previous studies/models (H¨urlimann et al. 2008; Rickenmann and Scheidl 2013; RAMMS v.1.7.0). Since these landslides are relatively deep in nature and during the slope failure, irrespective of type of trigger, entire loose material might not slide down, the depth of landslide is taken as only ¼ (thickness) in the run-out calculation. Further, a release area concept (for unchanneled flow or block release) was used for the run-out simulation. During the field visits, no specific flow channels (or gullies) were found on the landslide slopes except a few centimeters deep seasonal flow channels for S. N. 5 and S.N. 15 landslides (Table 1). However, the data pertaining to the spatial-temporal pattern of discharge at these two landslides was not available. Therefore, the release area concept was chosen because it has been more appropriate when the flow path (e.g. gully) and its possible discharge on the slope is uncertain (RAMMS v.1.7.0).

4.0 RESULTS

4.1 Slope instability regime and parametric output

Out of the 44 landslides studied here, 31 are in meta-stable state ($1 \leq FS \leq 2$) and 13 in unstable state ($FS < 1$) (Fig. 4). Most of the unstable landslides are debris slides, whereas the majority of the meta-stable landslides are rock fall/rock avalanche. Debris slides constitute ~ 90 % and ~99 % of the total area and volume, respectively, of the unstable landslides. Notably, about ~70 % of the total human population along the study area resides in the vicinity (~500 m) of these unstable debris slides (Fig. 4). Rock falls/Rock avalanches constitute ~84 % and ~78 % of the area and volume, respectively, of the meta-stable landslides. Out of total 20 debris slides, 12 debris slides are found to be in unstable stage, whereas 8 in the meta-stable condition (Fig. 4). These 20 debris slides occupy ~$1.9 \pm 0.02 \times 10^6$ m^2 area and ~ $26 \pm 6 \times 10^6$ m^3 volume. When comparing the Factor of Safety (FS) with the Total Displacement (TD) and Shear Strain (SS), nonlinear poor correlation is achieved (Fig. 5). Since the TD and SS are a relatively good correlation (Fig. 5), only the TD is used further along with the FS. The TD ranges from 7.4± 8.9 cm to 95.5± 10 cm for the unstable debris slides and ~18.8 cm for meta-stable landslides

(Fig. 4). Out of 13 rockfalls, 1 belongs to the unstable state and 12 to the meta-stable state (Fig. 4). The TD varies from 0.4 to 80 cm with the maximum for Bara Kamba rockfall (S.N. 31). Out of 11 rock avalanches, 1 belongs to the unstable state and 10 to the meta-stable state (Fig. 4). The TD varies from 6.0 to 132.0 cm with the maximum for the Kandar rock avalanche (S.N. 25). Relatively higher TD is obtained by the rock fall and rock avalanche of the Lesser Himalaya Crystalline region (Fig. 4). The landslides of the Higher Himalaya Crystalline (HHC), Kinnaur Kailash Granite (KKG) and Tethyan Sequence (TS), despite being only 17 out of the total 44 landslides, constituted ~ 67 % and ~ 82 % of the total area and total volume of the landslides.

The Factor of Safety (FS) of debris slides is found to be relatively less sensitive to the change in the value of input parameters than the Total Displacement (TD) (Fig. 6). In case of Akpa (Fig. 6a) and Pangi landslide (Fig. 6b), soil friction and field stress have more influence on the FS. However, for TD, field stress, elastic modulus and Poisson's ratio of the soil are relatively more controlling parameters. The FS and TD of the Barauni Gad landslide (Fig. 6c) are relatively more sensitive to soil cohesion and 'mi' parameter. Therefore, it can be inferred that the FS of debris slides is more sensitive to soil friction and field stress, whereas TD is mostly controlled by the field stress and deformation parameters i.e, elastic modulus and Poisson's ratio. Similar to the debris slides, the FS of rock falls and rock avalanche are found to be relatively less sensitive than TD to the change in the value of input parameters (Fig. 7). Tirung Khad rock fall (Fig. 7a) and Baren Dogri rock avalanche (Fig. 7b) show dominance of 'mi' parameter and field stress in the FS as well as in TD. In case of Chagaon rock fall (Fig. 7c), Poisson's ratio and UCS have relatively more influence on FS and TD. Thus, it can be inferred that the rock fall/rock avalanche are more sensitive to 'mi' parameter and field stress.

4.2 Potential landslide damming

Based on the MOI, out of total 44 landslides, 5 (S.N. 5, 7, 14, 15, 19) are observed to be in the formation domain, 15 in uncertain domain, and 24 in non-formation domain (Fig. 8a). Thefive landslides that have potential to dam the river in case of slope failure comprise ~26.3 ± 6.7 x 10^6 m^3 volume (Fig. 9 a-e). In terms of temporal stability (or durability), out of these five landslides, only one landslide (S.N. 5) is noted to attain the 'uncertain' domain, whereas the remaining four show 'instability' (Fig. 8b,d). The lacustrine deposit in the upstream of Akpa landslide (S.N. 5) in Fig. 9a shows signs of landslide damming in the past (Fig. 10). The 'uncertain' temporal stability indicates that the landslide dam may be stable or unstable

depending upon the stream power and landslide volume, which in turn are dynamic factors and may change owing to the changing climate and/or tectonic event. The landslides that have been observed to form the landslide dam but are noted to be in temporally unstable category (S.N. 7, 14, 15, 19) are still considerable owing to the associated risks of lake-impoundment and generation of secondary landslides. Urni landslide (S.N. 19) (Fig. 9e) that damaged the part of National Highway road (NH)-05 has already partially dammed the river since year 2016 and holds potential for the further damming (Kumar et al. 2019a). Apart from the S.N. 5 and S.N. 19 landslides, remaining landslides (S.N. 7, 14, 15) belong to the Higher Himalaya Crystalline (HHC) region that has been observed to accommodate many landslide dams and subsequent flash floods events in the geological past (Sharma et al. 2017).

4.3 Rainfall and Earthquake regime

In order to explain the spatio-temporal variation in rainfall, the topographic profile of the study area is also plotted along with the rainfall variation (Fig. 11a). The temporal distribution of rainfall is presented at annual, monsoonal i.e., Indian Summer Monsoon (ISM): June-September and non-monsoonal i.e., Western Disturbance (WD): Oct-May (Fig. 11b-d) level. Rainfall data of the years 2000-2019 revealed a relative increase in the annual rainfall since the year 2010 (Fig. 11b). The Kalpa region (orographic barrier) received relatively more annual rainfall than the Rampur, Nachar and Moorang regions throughout the time period, except the year 2017. The rainfall dominance at Kalpa is more visible in the non-monsoonal season (Fig. 11d). This difference may be due to the orographic influence on the saturated winds of the WD (Dimri et al. 2015). Further, the rainfall during the monsoon season that was dominant at the Rampur region till year 2012 gained dominance at Kalpa region since the year 2013 (Fig. 11c).

Extreme rainfall events of June 2013 that resulted in the widespread slope failure in the NW Himalaya also caused landslide damming at places (National Disaster Management Authority, Govt. of India, 2013; Kumar et al. 2019a). Similar to the year 2013, the years 2007, 2010 and 2019 also witnessed enhanced annual rainfall and associated flash floods and/or landslides in the region (hpenvis.nic.in, retrieved on March 1, 2020; sandrp.in, retrieved on March 1, 2020). However, the contribution of the ISM and WD associated rainfall was variable in those years (Fig. 11). Such frequent but inconsistent rainfall events that possess varied (temporally) dominance of the ISM and WD are noted to owe their occurrence to the El-Nino Southern Oscillation (ENSO), Equatorial Indian Ocean Circulation (EIOC), and planetary warming (Gadgil et al. 2007; Hunt et al. 2018). The orographic setting is noted to act as a main local

factor as evident from the relatively more rainfall (total precipitation=1748±594 mm/yr.) at Kalpa region (orographic barrier) in the non-monsoon and monsoon season from the year 2010 onwards (Fig. 11). Prediction of the potential landslide damming sites in the region revealed that four (S.N. 7, 14, 15, 19) out of five landslides that are predicted to be able to form dams belong to this orographic barrier region. Therefore, in view of the prevailing rainfall trend since the year 2010, regional factors, discussed above, and orographic setting, precipitation triggered slope failure events may be expected in the future. Such slope failure events, if they occur, at the predicted landslide damming sites may certainly dam the river.

The seismic pattern revealed that the region has been hit by 1662 events during the years 1940-2019 with the epicenters located in and around the study area (Fig. 12a). However, ~99.5 % of these earthquake events had a magnitude of less than 6.0 and only 8 events are recorded in the range of 6.0 to 6.8 M_s (International Seismological Centre 2019). Out of these 8 events, only one event i.e., at 6.8 M_s (19^{th} Jan. 1975), has been noted to induce widespread slope failures in the study area (Khattri et al. 1978). The majority of the earthquake events in the study area occurred in the vicinity of the N-S oriented trans-tensional Kaurik - Chango Fault (KCF) that accommodated the epicenter of 19^{th} Jan. 1975 earthquake (Hazarika et al. 2017; http://www.isc.ac.uk/iscbulletin/search/catalogue/, retrieved on 02 March 2020). About 95% of the total 1662 events had their focal depth within 40 km (Fig. 12b). Such a relatively low magnitude - shallow seismicity in the region has been related to the Main Himalayan Thrust (MHT) decollement as a response to the relatively low convergence (~14±2 mm/yr) of India and Eurasia plates in the region (Bilham 2019) (Fig. 12c). Further, the arc (Himalaya)-perpendicular Delhi-Haridwar ridge that is under thrusting the Eurasian plate in this region has been observed to be responsible for the spatially varied *low* seismicity in the region (Hazarika et al. 2017). Thus, though the study area has been subjected to frequent earthquakes, chances of earthquake-triggered landslides have been relatively low in comparison to rainfall-triggered landslides and associated landslide damming. For this reason and the lack of reliable dynamic load of major earthquake event, we have performed the *static* modelling in the present study. However, we intend to perform the *dynamic* modelling in the near future if the reliable dynamic load data will be available.

4.4 Run-out analysis

All five landslides (S.N. 5, 7, 14, 15, 19 in Fig. 9) that are predicted to form potential landslide dams in case of slope failure were also used for the run-out analysis to evaluate expected runout distances in the event of reactivation and failure in the future. Results are as follows;

4. 4.1 Akpa landslide (S.N. 5)

Though it is difficult to ascertain the extent to which the predicted debris flow might contribute in the river blockage, it will certainly block the river in view of ~38 m high debris material with ~50 m wide run-out across the channel in this narrow part of river valley (Fig. 9a) even at maximum value of coefficient of friction (i.e., μ =0.3) (Fig. 13a). Notably, not only the run-out extent but flow height also decreases on increasing the friction value (Fig. 13a.1-13.a.3). The maximum friction takes into account the shear resistance by slope material and the bed-load on the river channel. However, apart from the frictional characteristics of run-out path, turbulence of a debris flow also controls its dimension and hence consequences like potential damming. Therefore, different values of turbulence coefficient (ξ) were used (Table 4). The resultant flow height (representing 9 sets of modeled debris flows obtained using μ=0.05, 0.1 and 0.3 and ξ= 100,200 and 300 m/s^2) attains its peak value i.e., 39.8± 4.0m at the base of central part of landslide (Fig. 14a).

4.4.2 Baren dogri landslide (S.N. 7)

At the maximum friction value (μ =0.4), the Baren dogri landslide would attain a peak value of flow height i.e., ~30 m at the base of central part of landslide (Fig. 13b). Similar to the valley configuration around the Akpa landslide (sec 4.4.1), the river valley attains a narrow/deep gorge setting here also (Fig. 9b). The maximum value of debris flow height obtained using the different μ and ξ values is 25.6 ± 2.1m (Fig. 14b). Flow material is also noted to attain more run-out in upstream direction of river (~1100 m) than in the downstream direction (~800 m). This spatial variability in the run-out length might exist due to the river channel configuration as river channel in upstream direction is relatively narrower than the downstream direction.

4.4.3 Pawari landslide (S.N. 14)

The Pawari landslide attains maximum flow height of ~20 m at the maximum friction of run-out path (μ=0.4) (Fig. 13c). The resultant debris flow that is achieved using the different values of μ and ξ parameters attains a peak value of 24.8 ± 2.7 m and decreases gradually with a run-out of ~1500 m in upstream and downstream direction (Fig. 14c). This landslide resulted in the relatively long run-out of ~1500 in the upstream and downstream direction. Apart from the

landslide volume that affects the run-out extent, valley morphology also controls it as evident from the previous landslides. The river channel in upstream and downstream direction from the landslide location is observed to be narrow (Fig. 9c).

4.4.4 Telangi landslide (S.N. 15)

The Telangi landslide would result in peak debris flow height of ~24 m at the maximum friction (μ=0.4) (Fig. 13d). On increasing the friction of run-out path, flow run-out decreased along the river channel but increased across the river channel resulting into possible damming. The debris flow after taking into account different values of μ and ξ parameters attains a peak value of 25.0± 4.0 m (Fig. 14d). Similar to Baren dogri landslide (S.N. 7), material attained more run-out in the upstream direction of river (~1800 m) than in the downstream direction (~600 m) ; this difference can be attributed to a narrower river channel in upstream than the downstream direction. The downstream side attains wider river channel due to the Main Central Thrust (MCT) fault in the proximity (Fig. 1). Since the Pawari and Telangi landslides (S.N 14 &15) are situated ~500 m from each other, their respective flow run-outs might mix in the river channel resulting into disastrous cumulative effect.

4.4.5 Urni landslide (S.N. 19)

The Urni landslide is predicted to attain a peak value of ~44 m of debris flow height at the maximum friction value (μ=0.4) (Fig. 13e). After considering different values of μ and ξ parameters, the debris flow would attain a height of 26.3± 1.8 m (Fig. 14e). The relatively wider river channel in the downstream direction (Fig. 9e) results in longer run-out in downstream direction than in the upstream.

5.0 DISCUSSION

This study aimed to determine the potential landslide damming sites in the Satluj River valley, NW Himalaya. In order to achieve this objective, 44 active landslides were considered. First, slope stability evaluation of all the slopes, at these landslides sites was performed alongwith the parametric evaluation. Then the geomorphic indices, i.e., Morphological Obstruction Index (MOI) and Hydro-morphological Dam Stability Index (HDSI), were used to predict the formation of potential landslide dams and their subsequent stability. Rainfall and earthquake regime were also explored in the study area. Finally, run-out analysis was performed for those landslides that have been observed to form the potential landslide dam.

The MOI revealed that out of 44 active landslides in the Satluj valley, five (S.N. 5, 7, 14, 15, 19) have the potential to form the landslide dam (Fig. 8, 9). On evaluating the stability of such potential dam sites using the HDSI, one landslide (S.N. 5) is predicted to attain an 'uncertain' domain (5.74<HDSI<7.44) in terms of dam stability. The uncertain term implies that the resultant dam may be stable or unstable depending upon the landslide/dam volume, upstream catchment area (or water discharge) and slope gradient (sec 3.3). Since this landslide (S.N.5) presents clear signs of having already formed a dam in the past, as indicated by the alternating fine-coarse layered sediment deposit (or lake deposit) in the upstream region (Fig. 10), recurrence is expected in the future. Further, run-out analysis of this landslide has predicted a 39.8± 4.0m high debris flow in the event of failure that will block the river completely (Fig. 13a, 14a). However, the durability of the blocking cannot be ascertained as it will depend on the volume of landslide that will be retained in the channel and river discharge.

The remaining four landslides (S.N. 7, 14, 15, 19), though showing instability i.e., HDSI <5.74 at present, may form dams in the near future as the region accommodating these landslides has been affected by such damming and subsequent flash floods in the past (Sharma et al. 2017). The last one of these i.e., S.N. 19 (Urni landslide) has already dammed the river partially and holds potential to completely block the river in near future (Kumar et al. 2019a). Run-out analysis of these landslides (S.N. 7, 14, 15, 19) has predicted 25.6 ± 2.1m, 24.8 ± 2.7m, 25.0± 4.0m and 26.3± 1.8m flow height, respectively that will result in temporary blocking of the river (Fig. 13,14). These findings of run-out indicate the blocking of river in the event of slope failure, irrespective of durability, despite the conservative depth as input because only ¼ of landslide thickness is used in the run-out analysis (sec. 3.5).

Stability evaluation of these five landslide slopes (S.N. 5, 7, 14, 15, 19) that have potential to form landslide dams revealed that one landslide (S.N.7) is meta-stable, while the other four belong to the unstable category (Fig. 4). Further, these four unstable landslide slopes are debris slides in nature. It is noteworthy to discuss the implications of FS<1. The Factor of Safety (FS) in the Shear Strength Reduction (SSR) approach is a factor by which the existing shear strength of material is divided to determine the critical shear strength at which failure occurs (Zienkiewicz et al. 1975; Duncan 1996). Since the landslide represents a failed slope i.e., critical shear strength > existing shear strength, FS<1 is justifiable. Further, the failure state of a slope in the FEM can be defined by different criteria; the FS of the same slope may vary a

little depending upon the usage of failure criteria and the convergence threshold (Abramson et al. 1996; Griffiths and Lane 1999).

The possible causes of instability (FS<1) may be steep slope gradient, rockmass having low strength, and joints. Three (S.N. 7, 14, 15) out of the five landslides that have potential to form dams belong to the tectonically active Higher Himalaya Crystalline (HHC). The notion of steep slope gradient cannot be generalized because the HHC accommodates voluminous (~10^5-10^7 m^3) landslides (Fig. 4). These deep seated landslides must require smooth slope gradient to accommodate the voluminous overburden. Further, the HHC comprises gneiss having high compressive strength and Geological Strength Index (Supplementary Table 2, Kumar et al. 2021), therefore the notion of low strength rockmass also may not be appropriate. However, the jointed rock mass that owes its origin to numerous small-scale folds, shearing, and faults associated with the active orogeny process can be considered as the main factor for relatively more instability of debris slide type landslides. Since, the study area is subjected to the varied stress regime caused by the tectonic structures (Vannay et al. 2004), thermal variations (Singh et al. 2015), and anthropogenic cause (Lata et al. 2015), joints may continue to develop and destabilize the slopes. Apart from this inherent factor like joints, external factors like rainfall and exhumation rate may also contribute to instability of these landslides. This region receives relatively more annual rainfall owing to orographic barrier setting (Fig. 11) and is subjected to relatively high exhumation rate of 2.0-4.5 mm/yr (Thiede et al. 2009).

Two landslides (S.N. 5, 19) that are also capable of forming potential landslide dams (Fig. 8, 9a; e) and are also unstable (FS<1) in nature (Fig. 4) do not belong to the HHC. The first landslide (S.N. 5) exists at the lithological contact of schist of the Tethyan Sequence and Kinnaur Kailash Granite rockmass. A regional normal fault, the Sangla Detachment (SD), passes through this contact. Some prior studies suggest that the SD is an outcome of reactivation of a former thrust fault that has resulted in intense rockmass shearing (Vannay et al. 2004; Kumar et al. 2019b). Owing to its location in the orographic interior region, hillslopes receive very low annual rainfall (Fig. 11) and thus have the least vegetation on the hillslopes in this region. The lack of vegetation on hillslopes has been observed to result in low shear strength of material and hence in the instability (Kokutse et al. 2016). Thus, lithological contrast, rockmass shearing, and lack of vegetation are thought to be the main reasons of instability of S.N. 5 landslide. The second landslide (S.N. 19) belongs to the inter-layered schist/gneiss rockmass of the Lesser Himalaya Crystalline (LHC) and is situated at the

orographic front where rainfall increases suddenly (Fig. 11). Further, this region is also subjected to the high exhumation rate of 2.0-4.5 mm/yr (Thiede et al. 2009). Therefore, lithological contrast, high rainfall and high exhumation rate are considered as the main reasons of instability of this landslide slope.

The landslides that are inferred not to result in the river damming are mostly in the LHC and Lesser Himalaya Sequence (LHS) region. These regions consist of a majority of the rock fall and rock avalanches that are generally of meta-stable category (Fig. 4). Despite the narrow valley setting, landslides in these regions may not form the potential landslide dam, at present, owing to the relatively small landslide volume. The possible causes of their meta-stability may be high compressive strength and geological strength index of gneiss (Kumar et al. 2021), dense vegetation on the hillslopes (Chawla et al. 2012), relatively less sheared rock mass in comparison to the HHC region, and relatively less decrease in land use/landcover (Lata et al. 2015). Maximum Total Displacement (TD) is also associated with the rock fall and rock avalanche of this region (Fig. 4).

In the parametric study, soil friction and in-situ stress are noted to affect the FS most in case of the debris slide, whereas the FS of rock fall and rock avalanche are mainly controlled by the 'm_i' and the in-situ stress. The 'm_i' is a GHB criteria parameter that is equivalent to the friction in the M-C criteria. For the TD of the debris slides, field stress, elastic modulus and Poisson's ratio, whereas for rock falls and rock avalanches, the 'm_i' parameter and in-situ stress played the dominant role (Fig. 6,7). Friction has been a controlling factor for the shear strength, and its decrease has been observed to result in the shear failure of slope material (Matsui and San 1992). Since rainfall plays an important role in decreasing the friction of slope material by changing the pore water pressure regime (Rahardjo et al. 2005), frequent extreme rainfall events in the study area since the year 2013 (Kumar et al. 2019a) amplify the risk of hillslope instability. Furthermore, the in-situ field stress that has been compressional and/or extensional owing to the orogenic setting in the region may also enhance the hillslope instability (Eberhardt et al. 2004; Vannay et al. 2004). Deformation parameters, e.g. elastic modulus and Poisson's ratio, are also observed to affect the displacement in slope models of the debris slides. Similar studies in other regions have also noted the sensitivity of the elastic modulus and Poisson's ratio on the slope stability (Zhang and Chen 2006).

The study area has been subjected to extreme rainfalls since the year 2010 and received widespread slope failures and flash-floods (Fig. 11b). Three (S.N. 7,14,15 in Fig. 9) out of five

potential landslide dams belong to the Higher Himalaya Crystalline (HHC) that receives relatively more rainfall (Fig. 11). Contrary to the along 'Himalayan' arc distribution of earthquakes, the study area has received most of the earthquakes around the N-S oriented Kaurik-Chango Fault (Fig. 12a). However, the only major earthquake event has been M_w 6.8 earthquake on 19th Jan. 1975 that resulted in the widespread landslides (Khattri et al. 1978). The low-magnitude recent seismicity in the region has been attributed to the northward extension of the Delhi-Haridwar ridge (Hazarika et al. 2019), whereas the shallow nature is attributed to the MHT ramp structure in the region that allows strain accumulation at shallow depth (Bilham 2019). Thus, earthquakes have not been a major landslide triggering process in the region in recent times. Finally, the word "active landslide" refers to the hillslope that is still subjected to the slope failures caused by the various factors. The word "landslide" can be perceived in the following three ways; pre-failure deformations, failure itself, and post-failure displacement (Terzaghi 1950; Cruden & Varnes, 1996; Hungr et al., 2014). Landslide slopes in this study pertain to the post-failure state that are categorized into "unstable" and "meta-stable" stages based on their existing FS. If an active landslide is not categorized as "unstable", it means that the existing slope geometry provides it a "meta-stable" stage that might transform into an unstable stage with time due to the stability controlling parameters (Sec. 4.1). Though the field visits were performed in different seasons to cover all the landslides along the study area, there might be a possibility of vegetation growth on the failed slopes, particularly in the LHC and LHS. However, the landslides in the LHC and LHS are mostly rockfall/rock avalanche type because of the deep gorge setting, whereas the vegetation growth generally requires the debris laden hillslopes. Nonetheless, such aspect will be explored in the future prospects. The HHC and the TS region are subjected to the semi-humid to semi-arid climate and hence the vegetation type is mostly scattered trees/shrubs. Therefore, such possibility might not exist in these regions.

A supplementary table involving all the details like landslides dimensions, factor of safety, and geomorphic indices output of each landslide is provided in the data repository (Kumar et al. 2021).

In view of the possible uncertainties in the predictive nature of the study, the following assumptions and simplifications were made;

- To account the effect the spatial variability in the slope geometry, 3D models have been in use for the last decade (Griffiths and Marquez 2007). However, the pre-requisite for

548 the 3D models involves the detailed understanding of slope geometry and material
549 variability in the subsurface that was not possible in the study area considering steep
550 and inaccessible slopes. Therefore, multiple 2D sections were chosen, wherever
551 possible. To account the effect of sampling bias and material variability, a range of
552 values of input parameters was used (sec. 4.1).

553 • Determination of the debris thickness has been a major problem in the landslide volume
554 measurement particularly in the steep, narrow river valleys of the NW Himalaya.
555 Therefore, the thickness was approximated by considering the relative altitude of the
556 ground on either side of the deposit, as also performed by Innes (1983). It was assumed
557 that the ground beneath the deposit is regular.

558 • The resultant dam volume could be different from the landslide volume due to the
559 entrainment, rockmass fragmentation, pore water pressure, size of debris particles, and
560 washout of landslide material by the river (Hungr and Evans 2004; Dong et al. 2011;
561 Yu et al. 2014). Therefore, dam volume is presumed to be equal to landslide volume
562 for the worst-case scenario (sec. 3.3). Stream power is manifested by the upstream
563 catchment area and local slope gradient in the geomorphic indices. It may also vary at
564 temporal scale owing to the temporally varying water influx from glaciers and
565 precipitation systems i.e., ISM and WD (Gadgil et al. 2007; Hunt et al. 2018). Though
566 our study is confined to the spatial scale at present, the findings remain subjected to the
567 change at temporal scale.

568 • The RAMMS model (Voellmy 1955; Salm 1993; Christen et al. 2010) requires the
569 calibrated friction and turbulence values for the run-out analysis. Though the previous
570 debris flow events have not left evidence in the study area owing to the convergence of
571 the landslide toes with the river channel, a range of μ and ξ values were used in the
572 study in view of the material type and run-out path characteristics.

573 Despite these uncertainties, studies such as this one are required to minimize the risk and
574 avert the possible disasters in the terrain where human population lives in the proximity of
575 unstable landslides.

576 **CONCLUSION**

577 Out of forty-four landslides that are studied in the Satluj valley in the NW Himalaya, five
578 landslides are noted to form the potential landslide dam, if failure occurs. Though the blocking
579 duration is difficult to predict, upstream and downstream consequences of these damming

events should be carefully considered as the region has witnessed many damming and flash floods in the past. These five landslides comprise a total landslide volume of 26.3± 6.7 M m^3. The slopes of four landslides (debris slides) out of these five are unstable, whereas the remaining one (rock avalanche) is meta-stable. Field observations and previous studies have noted the damming events by these landslides (or the region consisting these landslides) in the past also. Since the area is witnessing enhanced rainfall and flash floods since year 2010, findings of the run-out analysis that revealed 24.8 ± 2.7m to 39.8± 4.0m high material flow from these landslides become more crucial. The parametric analysis for the slope stability evaluation revealed that the angle of internal friction of soil or 'm_i' (equivalent to the angle of internal friction) of the rockmass, and *in-situ* field stress are the most controlling parameters for the stability of slopes.

ACKNOWLEDGEMENT

VK and IJ acknowledge the constructive discussion on the regional scale study with Prof. H.B. Havenith, Prof. D.V. Griffiths, and Prof. D.P. Kanungo. VG and RKB acknowledge the financial help through the project MOES/Indo-Nor/PS-2/2015. Authors are thankful to the RAMMS developer for the license. Authors are also grateful to Prof. A Joshua West (Editor), Prof. Xuanmei Fan (Associate Editor), and two anonymous reviewers for their insightful comments that improved the final manuscript.

Conflict of Interest

The authors declare that they have no conflict of interest.

Dataset Availability

The dataset is uploaded in the open access repository (*Mendeley data*) as Kumar et al. (2020).

Author contribution

VK conceived the idea and collected the field data. VK and IJ performed the laboratory analysis. All authors contributed to the dataset compilation, numerical simulation, and geomorphic interpretations. All authors contributed to the writing of the final draft.

REFERENCES

Abramson, L. W., Lee, T. S., Sharma, S. 1996. "Slope stability and stabilization methods". New York. Wiley.

609 Aydin, A. 2008."ISRM suggested method for determination of the Schmidt hammer rebound
610 hardness: revised version". *In: R. Ulusay (ed) The ISRM Suggested Methods for Rock*
611 *Characterization, Testing and Monitoring: 2007–2014*. Springer, Cham, pp. 25-33.
612 Barton, N. and Bandis, S. 1982."Effects of block size on the shear behavior of jointed rock".
613 *In: Proc. 23rd US symposium on rock mechanics*. American Rock Mechanics
614 Association, 739-760.
615 Barton, N. and Choubey, V. 1977."The shear strength of rock joints in theory and practice".
616 *Rock mechanics* 10(1-2):1-54.
617 Barton, N. R. 1972."A model study of rock-joint deformation. International journal of rock
618 mechanics and mining sciences". *Geomech. Abstr.* 9 (5): 579-602.
619 Barton, N. R. and Bandis, S. C. 1990."Review of predictive capabilities pf JRC-JCS model in
620 engineering practice". *In: Barton N and Stephansson O (ed) Rock Joints,* Rotterdam, pp.
621 603-610.
622 Bhasin, R. and Kaynia, A. M. 2004."Static and dynamic simulation of a 700-m high rock slope
623 in western Norway". *Engineering Geology* 71(3-4): 213-226.
624 Bilham, R. 2019."Himalayan earthquakes: a review of historical seismicity and early 21st
625 century slip potential". *Geological Society, London, Special Publications*. 483(1):423-
626 82.
627 Bowles, J. E. 1996.*Foundation Analysis and Design,5thed.*, McGraw-Hill, New York, pp. 750.
628 Braun, A., Cuomo, S., Petrosino, S., Wang, X. and Zhang, L., 2018. "Numerical SPH analysis
629 of debris flow run-out and related river damming scenarios for a local case study in SW
630 China". *Landslides* 15 (3), 535-550.
631 Cai, M., Kaiser, P. K., Tasaka, Y. and Minami, M. 2007."Determination of residual strength
632 parameters of jointed rock masses using the GSI system". *International Journal of Rock*
633 *Mechanics and Mining Sciences* 44(2): 247-265.
634 Chawla, A., Kumar, A., Lal, B., Singh, R.D. and Thukral, A.K. 2012."Ecological
635 Characterization of High Altitude Himalayan Landscapes in the Upper Satluj River
636 Watershed, Kinnaur, Himachal Pradesh, India". *Journal of the Indian Society of Remote*
637 *Sensing* 40(3): 519-539.
638 Cho, S. E. 2007."Effects of spatial variability of soil properties on slope stability". *Engineering*
639 *Geology* 92(3-4): 97-109.
640 Christen, M., Kowalski, J., Bartelt, P. 2010. "RAMMS: Numerical simulation of dense snow
641 avalanches in three-dimensional terrain". *Cold Regions Science and Technology*.63: 1-
642 14.
643 Corominas, J. and Mavrouli, J., 2011. "Living with landslide risk in Europe: Assessment,
644 effects of global change, and risk management strategies". *Documento tecnico, safeland.*
645 *7th Framework Programme Cooperation Theme,* 6.
646 Costa, J. E. and Schuster, R. L. 1988."The formation and failure of natural dams". *Geological*
647 *society of America bulletin* 100(7): 1054-1068.
648 Coulomb, C. A. 1776."An attempt to apply the rules of maxima and minima to several
649 problems of stability related to architecture". *Mémoires de l'Académie Royale des*
650 *Sciences* 7: 343-382.

Cruden, D. M. and Varnes, D. J. 1996. Landslides: investigation and mitigation. In: Landslide types and processes. Transportation Research Board, US National Academy of Sciences, Special Report, (247).

Dai, F.C., Lee, C.F., Deng, J.H. and Tham, L.G. 2005."The 1786 earthquake-triggered landslide dam and subsequent dam-break flood on the Dadu River, southwestern China". *Geomorphology* 65(3): 205-221.

Deere, D. U. and Miller, R. P. 1966."Engineering classification and index properties for intact rock". Illinois University at Urbana, USA.

Delaney, K. B. and Evans, S. G. 2015."The 2000 Yigong landslide (Tibetan Plateau), rockslide-dammed lake and outburst flood: review, remote sensing analysis, and process modelling". *Geomorphology* 246, 377-393.

Dimri, A.P., Niyogi, D., Barros, A.P., Ridley, J., Mohanty, U.C., Yasunari, T. and Sikka, D.R. 2015."Western disturbances: A review". *Reviews of Geophysics* 53(2): 225-246

Dong, J.J., Tung, Y.H., Chen, C.C., Liao, J.J. and Pan, Y.W. 2011."Logistic regression model for predicting the failure probability of a landslide dam". *Engineering Geology* 117(1): 52-61.

Duncan, J. M. 1996."State of art: limit equilibrium and finite element analysis of slopes". *Journal of Geotechnical Engineering Division,* ASCI 122 (7): 577-596.

Eberhardt, E., Stead, D. and Coggan, J. S. 2004."Numerical analysis of initiation and progressive failure in natural rock slopes—the 1991 Randa rockslide". *International Journal of Rock Mechanics and Mining Sciences* 41(1): 69-87.

Ermini, L. and Casagli, N. 2003."Prediction of the behaviour of landslide dams using a geomorphological dimensionless index". *Earth Surface Processes and Landforms* 28(1): 31-47.

Fan, X, Dufresne, A, Subramanian, SS, Strom, A, Hermanns, R, Stefanelli, CT, Hewitt, K, Yunus, AP, Dunning, S, Capra, L and Geertsema, M. 2020. "The formation and impact of landslide dams–State of the art". *Earth-Science Reviews,* 203:103116.

Fujisawa, K., Kobayashi, A. and Aoyama, S.2009."Theoretical description of embankment erosion owing to overflow". *Geotechnique* 59(8): 661-671.

Gadgil, S., Rajeevan, M. and Francis, P.A. 2007."Monsoon variability: Links to major oscillations over the equatorial Pacific and Indian oceans". *Current Science*. 93(2):182-94.

Griffiths, D. V. and Lane, P. A. 1999."Slope stability analysis by finite elements". *Geotechnique* 49(3): 387-403.

Griffiths, D. V. and Marquez, R. M. 2007."Three-dimensional slope stability analysis by elasto-plastic finite elements". *Geotechnique* 57(6): 537-546.

Gupta, V. and Sah, M. P. 2008."Impact of the trans-Himalayan landslide lake outburst flood (LLOF) in the Satluj catchment, Himachal Pradesh, India". *Natural Hazards* 45(3): 379-390.

Gupta, V. Nautiyal, H., Kumar, V., Jamir, I., and Tandon, R. S. 2016."Landslides hazards around Uttarkashi Township, Garhwal Himalaya, after the tragic flash flood in June 2013". *Natural Hazards* 80: 1689-1707

Huffman, G.J., Bolvin, D.T., Nelkin, E.J. and Adler, R.F. 2016. "TRMM (TMPA) Precipitation L3 1 day 0.25 degree x 0.25 degree V7, Edited by Andrey Savtchenko, Goddard Earth

Sciences Data and Information Services Center (GES DISC)", Accessed: 05 April 2020, 10.5067/TRMM/TMPA/DAY/7.
Hungr, O., Leroueil, S., and Picarelli, L. 2014. "The Varnes classification of landslide types, an update". *Landslides* 11 (2): 167-194.
Hürlimann, M., Rickenmann, D., Medina, V. and Bateman, A. 2008."Evaluation of approaches to calculate debris-flow parameters for hazard assessment". *Eng Geol* 102:152–163
Havenith, H.B., Torgoev, I. and Ischuk, A. 2018."Integrated Geophysical-Geological 3D Model of the Right-Bank Slope Downstream from the Rogun Dam Construction Site, Tajikistan". *International Journal of Geophysics* 1-17.
Hazarika, D., Wadhawan, M., Paul, A., Kumar, N. and Borah, K. 2017."Geometry of the Main Himalayan Thrust and Moho beneath Satluj valley, northwest Himalaya: Constraints from receiver function analysis". *Journal of Geophysical Research: Solid Earth*. 122(4):2929-45.
Hoek, E. and Brown, E.T. 1997."Practical estimates of rock mass strength". *International Journal of Rock Mechanics and Mining Science* 34(8):1165-1186
Hoek, E. and Diederichs, M.S. 2006."Empirical estimation of rock mass modulus". *International Journal of Rock Mechanics and Mining Sciences*43 (2): 203-15.
Hoek, E., Kaiser, P.K. and Bawden, W.F. 1995.*Support of Underground Excavations in Hard Rock*. Rotterdam: A. A. Alkema.
Hungr, O. and Evans, S.G. 2004."Entrainment of debris in rock avalanches: an analysis of a long run-out mechanism". *Geological Society of America Bulletin* 116(9-10): 1240-1252.
Hungr, O., Morgan, G.C. and Kellerhals, R. 1984."Quantitative analysis of debris torrent hazards for design of remedial measures". *Can Geotech J* 21:663–677
Hunt, K.M., Turner, A.G. and Shaffrey, L.C. 2018."The evolution, seasonality and impacts of western disturbances". *Quarterly Journal of the Royal Meteorological Society*. 144(710):278-90.
Hutter, K., Svendsen, B. and Rickenmann, D. 1994. "Debris flow modelling: a review". *Continuum mechanics and thermodynamics* 8: 1-35.
Innes, J. L. 1983."Debris flows". *Progress in Physical Geography* 7(4): 469–501.
IS: 2720 (Part 10)–1991. "Method of test for soils: Determination of unconfined compressive strength". *In: Bureau of Indian Standards, Delhi, India*.
IS: 2720 (Part 13)–1986. "Method of test for soils: Direct shear test". *In: Bureau of Indian Standards, New Delhi, India*.
IS: 2720 (Part 4)–1985. "Methods of test for soils: Grain size analysis". *In: Bureau of Indian Standards, New Delhi, India.*
IS: 9143-1979. "Method for the determination of unconfined compressive strength of rock materials". *In: Bureau of Indian Standards, New Delhi, India.*
Jamir, I., Gupta, V., Kumar, V. and Thong, G.T. 2017."Evaluation of potential surface instability using finite element method in Kharsali Village, Yamuna Valley, Northwest Himalaya". *Journal of Mountain Science* 14(8): 1666-1676.
Jamir, I., Gupta, V., Thong, G.T. and Kumar, V. 2019."Litho-tectonic and precipitation implications on landslides, Yamuna valley, NW Himalaya". *Physical Geography* 41(4) 365-388.

738 Jang, H.S., Kang, S.S. and Jang, B.A. 2014."Determination of joint roughness coefficients
739 using roughness parameters". *Rock mechanics and rock engineering* 47(6): 2061-73.
740 Jing, L. 2003."A review of techniques, advance and outstanding issues in numerical modelling
741 for rock mechanics and rock engineering". *International Journal of Rock Mechanics and*
742 *Mineral Science* 40:283-353.
743 Khattri, K., Rai, K., Jain, A.K., Sinvhal, H., Gaur, V.K. and Mithal, R.S. 1978."The Kinnaur
744 earthquake, Himachal Pradesh, India, of 19 January, 1975". *Tectonophysics*. 49(1-2):1-
745 21.
746 Kokutse, N.K., Temgoua, A.G.T. and Kavazović, Z. 2016."Slope stability and vegetation:
747 Conceptual and numerical investigation of mechanical effects". *Ecological Engineering*
748 86: 146–153.
749 Kumar, V., Gupta, V. and Jamir, I. 2018."Hazard Evaluation of Progressive Pawari Landslide
750 Zone, Kinnaur, Satluj Valley, Higher Himalaya, India". *Natural Hazards* 93: 1029-1047.
751 Kumar, V., Gupta, V., Jamir, I. and Chattoraj, S.L. 2019a."Evaluation of potential landslide
752 damming: Case study of Urni landslide, Kinnaur, Satluj valley, India". *Geosci. Front.*
753 10(2): 753-767.
754 Kumar, V., Gupta, V. and Sundriyal, Y.P. 2019b."Spatial interrelationship of landslides, litho-
755 tectonics, and climate regime, Satluj valley, Northwest Himalaya". *Geol. J.* 54: 537–551.
756 Kumar, V., Jamir, I., Gupta, V. and Bhasin, R.K. 2021. "Dataset used to infer regional slope
757 stability, NW Himalaya". *Mendeley Data.* DOI: 10.17632/jh8b2rh8nz.2
758 Kundu, B., Yadav, R.K., Bali, B.S., Chowdhury, S. and Gahalaut, V.K. 2014."Oblique
759 convergence and slip partitioning in the NW Himalaya: Implications from GPS
760 measurements." *Tectonics* 33: 2013-2024.
761 Lata, R., Rishi, S., Talwar, D. and Dolma, K. 2015."Comparative Study of Landuse Pattern in
762 the Hilly Area of Kinnaur District, Himachal Pradesh, India". *International Journal of*
763 *Innovative Science, Engineering & Technology* 2(4): 559-565.
764 Li, D.Q., Qi, X.H., Cao, Z.J., Tang, X.S., Phoon, K.K. and Zhou, C.B. 2016."Evaluating slope
765 stability uncertainty using coupled Markov chain". *Computers and Geotechnics*73:72-82.
766 Li, T., Schuster, R.L. and Wu, J. 1986."Landslide dams in south-central China". *In: Proc.*
767 *Landslide dams: processes, risk, and mitigation*, ASCE Convention, Washington,146-
768 162.
769 Li, M.H., Sung, R.T., Dong, J.J., Lee, C.T., and Chen, C.C.2011. "The formation and breaching
770 of a short-lived landslide dam at Hsiaolin village, Taiwan-Part II: Simulation of debris
771 flow with landslide dam breach". *Engineering Geology* 123: 60-71.
772 Martha, T.R., Kerle, N., Jetten, V., van Westen, C.J. and Kumar, K.V. 2010."Landslide
773 volumetric analysis using Cartosat-1-derived DEMs". *IEEE Geoscience and remote*
774 *sensing letters* 7(3): 582-586.
775 Matsui, T. and San, K.C. 1992."Finite element slope stability analysis by shear strength
776 reduction technique". *Soils and foundations* 32(1): 59-70.
777 Mohr, O. 1914."Abhandlungen aus dem Gebiete der Technischen Mechanik" (2nd ed). Ernst,
778 Berlin.
779 NDMA: National Disaster Management Authority.2013. Annual report, Government of India,
780 Delhi.

781 Nian, T.K., Chen, G.Q., Wan, S.S. and Luan, M.T. 2011."Non-convergence Criterion on Slope
782 Stability FE Analysis by Strength Reduction Method". *Journal of Convergence*
783 *Information Technology* 6:78-88.
784 O'Brien, J.S., Julien, P.Y. and Fullerton, W.T. 1993."Two-dimensional water flood and mud
785 flood simulation". *J Hydraul Eng* 119:244–260.
786 Parkash, S. 2011."Historical records of socio-economically significant landslides in India". *J*
787 *South Asia Disaster Studies* 4(2): 177-204.
788 Rahardjo, H., Lee, T.T., Leong, E.C. and Rezaur, R.B. 2005."Response of a residual soil slope
789 to rainfall". *Canadian Geotechnical Journal* 42(2): 340-351.
790 Rickenmann, D. 2005."Runout prediction methods". *In: Jakob M, Hungr O (eds) Debris-flow*
791 *hazards and related phenomena*. Praxis/Springer, Berlin/Heidelberg, pp. 305–324.
792 Rickenmann, D., and Scheidl, C. 2013.**"**Debris-Flow Runout and Deposition on the Fan".*M.*
793 *Schneuwly-Bollschweiler et al. (eds.), Dating Torrential Processes on Fans and Cones,*
794 *Advances in Global Change Research* 47, DOI 10.1007/978-94-007-4336-6 5
795 Ruiz-Villanueva, V., Allen, S., Arora, M., Goel, N. K. and Stoffel, M. 2016."Recent
796 catastrophic landslide lake outburst floods in the Himalayan mountain range". *Progress*
797 *in Physical Geography* 41 (1): 3-28.
798 Salm, B., 1993. "Flow, flow transition and runout distances of flowing avalanches". *Ann.*
799 *Glaciol*. 18: 221–226.
800 Sharma, S., Shukla, A.D., Bartarya, S.K., Marh, B.S. and Juyal, N. 2017."The Holocene floods
801 and their affinity to climatic variability in the western Himalaya, India". *Geomorphology*
802 290: 317–334.
803 Sharma, K. K. 1977."A contribution to the geology of Satluj Valley, Kinnaur, Himachal
804 Pradesh, India". *CollquesInternationaux du CNRS* 268: 369-378.
805 Singh, D., Gupta, R.D. and Jain, S.K. 2015."Statistical analysis of long term spatial and
806 temporal trends of temperature parameters over Sutlej river basin, India". *J. Earth Syst.*
807 *Sci*. 124 (1): 17-35.
808 Stefanelli, C.T., Segoni, S., Casagli, N. and Catani, F. 2016."Geomorphic indexing of landslide
809 dams evolution". *Engineering Geology* 208: 1-10.
810 Takahashi, T. And Nakagawa, H. 1993."Flood and debris flow hydrograph due to collapse of
811 a natural dam by overtopping". *In: Proc. Hydraulic Engineering, Japan*, 37: 699-704.
812 Terzaghi, K. 1950. "Mechanism of Landslides". *In: Application of Geology to Engineering*
813 *Practice. Geol. Soc. Am* 83-123.
814 Thiede, R.C., Ehlers, T.A., Bookhagen, B. and Strecker, M.R. 2009."Erosional variability
815 along the northwest Himalaya". *Journal of Geophysical Research: Earth Surface* 114
816 F101015.
817 Vannay, J.C., Grasemann, B., Rahn, M., Frank, W., Carter, A., Baudraz, V. and Cosca, M.
818 2004."Miocene to Holocene exhumation of metamorphic crustal wedges in the NW
819 Himalaya: Evidence for tectonic extrusion coupled to fluvial erosion". *Tectonics* 23
820 TC1014.
821 Voellmy, A. 1955. "On the destructive force of avalanches", *Translation No. 2.* Avalanche
822 Study Center, United States Department of Agriculture, USA.
823 Wong, F.S. 1984."Uncertainties in FE modelling of slope stability". *Computers & structures*
824 19(5-6): 777-791.

825 Wulf, H., Bookhagen, B. and Scherler, D. 2012."Climatic and geologic controls on suspended
826 sediment flux in the Sutlej River Valley, western Himalaya". *Hydrology and Earth*
827 *System Sciences* 16(7): 2193-2217.
828 Yu, G., Zhang, M., Chen, H., 2014. "The dynamic process and sensitivity analysis for debris
829 flow". *In: Sassa, K., Canuti, P., Yin, Y. (Eds.), Landslide Science for a Safer*
830 *Geoenvironment*. Springer.
831 Zhang, P. W. and Chen, Z. Y. 2006."Influences of soil elastic modulus and Poisson's ratio on
832 slope stability". YantuLixue (*Rock and Soil Mechanics*) 27(2): 299-303.
833 Zienkiewicz, O. C., Humpheson, C. and Lewis, R. W. 1975."Associated and non-associated
834 viscoplasticity and plasticity in soil mechanics". *Geotechnique* 25(4): 671-689.

835 **LIST OF FIGURES AND TABLES**

836 **Fig. 1** Geological setting. WGC: Wangtu Gneissic Complex. The red dashed circle in the inset
837 represents the region within 100 km radius from the Satluj River (marked as blue line) that
838 was used to determine the earthquake distribution in the area. Yellow lines represent the
839 regional faults in the region. KCF in inset refers to Kaurik-Chango Fault. The numbers 1-
840 44 refer to serial number of landslides in Table 1.

841 **Fig. 2** Field photographs of some of the landslides (a) Khokpa landslide (**S.N.1**); (b) Akpa_III
842 landslide (**S.N. 5**); (c) Rarang landslide (**S.N. 6**); (d) Pawari landslide (**S.N.14**); (e) Urni
843 landslide (**S.N.19**); (f) Barauni Gad_I_S landslide (**S.N. 38**). Black circle in the pictures
844 that encircles the vehicle is intended to represent the relative scale.

845 **Fig. 3** The FEM configuration of some of the slope models. S.N. refers to the serial no. of
846 landslides in Table 1. The joint distribution in all the slopes was parallel-statistical with
847 the normal distribution of joint spacing.

848 **Fig. 4** The FEM analysis of all forty-four landslides. Grey bar in the background highlights
849 the Higher Himalaya Crystalline (HHC) region that comprises relatively more unstable
850 landslides, landslide volume and human population..TS, KKG, HHC, LHC and LHS are
851 Tethyan Sequence, Kinnaur Kailash Granite, Higher Himalaya Crystalline, Lesser
852 Himalaya Crystalline and Lesser Himalaya Sequence, respectively.

853 **Fig. 5** Relationship of Factor of Safety (FS), Total Displacement (TD) and Shear Strain (SS).
854 DS, RF, and RA refer to Debris slide, rock fall and rock avalanche, respectively.

855 **Fig. 6** Parametric analysis of debris slides. (a) Akpa_III (S.N. 5); (b) Pangi_III (S.N. 13); (c)
856 Barauni Gad_I_S (S.N. 38). S. N. refers to the serial no. of landslides in Table 1.

Fig. 7 Parametric analysis of rockfall/rock avalanche. (a) Tirung khad (S.N. 2); (b) Baren Dogri (S.No. 7); (c) Chagaon_II (S.N. 21).

Fig. 8 Landslide damming indices (a) Morphological Obstruction Index (MOI); (b) Hydro-morphological dam stability index (HDSI); (c) Landslides vs. MOI; (d) Landslides vs. HDSI.

Fig. 9 Potential landslide damming locations. (a) Akpa_III landslide; (b) Baren dogri landslide; (c) Pawari landslide; (d) Telangi landslide; (e) Urni landslide. Red dashed-arrow represents the direction of river flow.

Fig. 10 Field signatures of the landslide damming near Akpa_III landslide. (a) Upstream view of Akpa landslide with lacustrine deposit at the left bank; (b) enlarged view of the lacustrine deposit with an arrow indicating the lacustrine sequence; (c) alternating fine-coarse sediments. F and C refer to fine (covered by yellow dashed lines) and coarse (covered by green dashed lines) sediments, respectively.

Fig. 11 Rainfall distribution. (a) Topographic profile; (b) annual rainfall; (c) monsoonal (June-Sep.) rainfall; (d) non-monsoonal (Oct.-May) rainfall. Green bars represent the years of relatively more rainfall resulting into the flash floods, landslides and socio-economic loss in the region. (i):hpenvis.nic.in, retrieved on March 1, 2020; Department of Revenue, Govt. of H.P. (ii): hpenvis.nic.in, retrieved on March 1, 2020.(iii): Kumar et al., 2019a;ndma.gov.in, retrieved on march 1, 2020 (iv):sandrp.in, retrieved on march 1, 2020.The numbers 1-44 refer to serial number of the landslides.

Fig. 12 Earthquake distribution. (a) Spatial variation of earthquakes. The transparent circle represents the region within 100 km radius from the Satluj River (blue line). The black dashed line represents the seismic dominance around the Kaurik-Chango fault;(b) earthquake magnitude vs. focal depth. The red dashed region highlights the concentration of earthquakes within 40 km depth; (c) Cross section view (Based on Hazarika et al. 2017; Bilham 2019). Red dashed circle represents the zone of strain accumulation caused by the Indian and Eurasian plate collision (Bilham 2019). ISC: International Seismological Centre. HFT: Himalayan Frontal Thrust.

Fig. 13 Results of the run-out analysis. μ refers to coefficient of friction.

886 **Fig. 14** Results of run-out analysis at different values of μ and ξ. μ and ξ refer to coefficient of
887 friction and turbulence, respectively.

888 **Table 1** Details of the landslides used in the study.

889 **Table 2** Details of the satellite imagery.

890 **Table 3** Criteria used in the Finite Element Method (FEM) analysis.

891 **Table 4** Details of input parameters used in the run-out analysis.

Table 1 Details of landslides used in the study.

S.N.	Landslide location	Latitude/ Longitude	Type	Area[1], m^2	Volume[2], m^3	Human population[3]	Litho-tectonic division
1	Khokpa	31°35'18.9"N 78°26'28.6"E	Debris slide	21897± 241	43794± 18361	373	Tethyan Sequence (TS)
2	Tirung Khad	31°34'50.4"N 78°26'20.5"E	Rockfall	28537± 314	14269± 9055	0	
3	Akpa _I	31°34'57.1"N 78°24'30.6"E	Rock avalanche	963051± 10594	1926102± 807515	0	TS-KKG
4	Akpa_II	31°35'2.2"N 78°23'25.4"E	Rock avalanche	95902± 1055	143853± 40734	470	Kinnaur Kailash Granite (KKG)
5	Akpa_III	31°34'54.5"N 78°23'2.4"E	Debris slide	379570± 4175	7591400± 3182681	1617	
6	Rarang	31°35'58.7"N 78°20'39.1"E	Rockfall	4586± 50	4586± 1923	848	Higher Himalaya Crystalline (HHC)
7	Baren Dogri	31°36'23.6"N 78°20'23.1"E	Rock avalanche	483721± 5321	2418605±421561	142	
8	Thopan Dogri	31°36'12.3"N 78°19'50.4"E	Rockfall	55296± 608	165888± 46974	103	
9	Kashang Khad_I	31°36'5.0"N 78°18'44.4"E	Debris slide	113054± 1244	169581± 48019	103	
10	Kashang Khad_II	31°35'58.3"N 78°18'34.0"E	Rockfall	27171± 299	40757± 11541	103	
11	Pangi _I	31°35'36.4"N 78°17'36.4"E	Debris slide	30112± 331	45168± 12790	1389	
12	Pangi _II	31°35'38.9"N 78°17'12.2"E	Debris slide	59436± 654	118872± 49837	1389	
13	Pangi _III	31°34'38.9"N 78°16'55.6"E	Debris slide	75396± 829	188490± 32854	7	
14	Pawari	31°33'49.8"N 78°16'28.6"E	Debris slide	320564± 3526	1602820± 279370	4427	
15	Telangi	31°33'7.0"N 78°16'37.2"E	Debris slide	543343± 5977	13583575± 2367608	6817	

16	Shongthong	31°31'13.0"N 78°16'17.0"E	Debris slide	5727± 63	11454± 2464	388	
17	Karchham	31°30'12.4"N 78°11'30.8"E	Rock avalanche	28046± 309	56092± 23516	0	
18	Choling	31°31'17.0"N 78° 8'4.9"E	Debris slide	20977± 231	20977± 8795	0	Lesser Himalaya Crystalline (LHC)
19	Urni	31°31'8.0"N 78° 7'42.2"E	Debris slide	112097± 1233	1120970± 469965	500	
20	Chagaon_I	31°30'55.9"N 78° 6'52.0"E	Rockfall	3220± 35	3220± 1350	0	
21	Chagaon_II	31°30'57.9"N 78° 6'47.7"E	Rockfall	11652± 128	11652± 4885	0	
22	Chagaon_III	31°31'3.0"N 78° 6'21.4"E	Debris slide	42141± 464	168564± 70670	1085	
23	Wangtu_U/s	31°32'4.8"N 78° 3'5.0"E	Rock avalanche	211599± 2328	317399± 89876	17	
24	Wangtu D/s__1	31°33'27.7"N 77°59'43.7"E	Debris slide	4655± 51	9310± 3903	71	
25	Kandar	31°33'43.7"N 77°59'54.9"E	Rock avalanche	151128± 1662	302256± 126720	186	
26	Wangtu D/s_ 2	31°33'38.9"N 77°59'29.9"E	Debris slide	8004± 88	16008± 6711	71	
27	Agade	31°33'52.3"N 77°58'3.5"E	Debris slide	9767± 107	14651± 4149	356	
28	Punaspa	31°33'37.6"N 77°57'31.5"E	Debris slide	3211± 35	3211± 1346	343	
29	Sungra	31°33'58.8"N 77°56'49.6"E	Debris slide	5560± 61	11120± 4662	2669	
30	Chota Kamba	31°33'39.2"N 77°54'39.0"E	Rock avalanche	197290± 2170	591870± 167597	401	
31	Bara Kamba	31°34'10.4"N 77°52'56.7"E	Rockfall	36347± 400	18174± 7619	564	
32	Karape	31°33'44.9"N 77°53'13.9"E	Debris slide	50979± 561	50979± 21373	1118	
33	Pashpa	31°34'40.2"N 77°50'53.0"E	Rockfall	16079± 171	8040± 3371	29	
34	Khani Dhar_I	31°33'43.4"N 77°48'52.5"E	Rock avalanche	218688± 2406	874752± 366738	0	
35	Khani Dhar_II	31°33'26.3"N 77°48'35.8"E	Rock avalanche	146994± 1617	734970± 248125	0	
36	Khani Dhar_III	31°33'20.1"N 77°48'27.8"E	Rock avalanche	20902± 230	62706± 17756	0	
37	Jeori	31°31'58.8"N 77°46'18.2"E	Rock avalanche	93705± 1031	93705± 39286	0	
38	Barauni Gad_I_S	31°28'56.6"N 77°41'40.4"E	Debris slide	63241± 696	758892± 111620	236	LHC-LHS
39	Barauni Gad_I_Q	31°29'00.0"N 77°41'38.0"E	Debris slide	59273± 652	711276± 104616	0	Lesser Himalaya

40	Barauni Gad_II	31°28'43.9"N 77°41'24.6"E	Rockfall	6977± 77	3489± 1463	0	Sequence (LHS)
41	Barauni Gad_III	31°29'5.6"N 77°41'23.7"E	Rockfall	33115± 364	33115± 13883	0	
42	D/s Barauni Gad_I	31°28'24.9"N 77°41'8.4"E	Rockfall	19101± 210	19101± 8008	0	
43	D/s Barauni Gad_II	31°28'25.5"N 77°40'56.7"E	Rockfall	21236± 234	21236± 8903	0	
44	D/s Barauni Gad_III	31°28'7.4"N 77°40'42.4"E	Rockfall	15632± 172	15632± 6554	0	

[1]Error (±) caused by GE measurement (1.06 %).

[2]Error (±) is an outcome of multiplication of area ± error and thickness ± error. Thickness error (Std. dev.) corresponds to averaging of field based approximated thickness.

[3]The human population is based on census 2011, Govt. of India. The villages/town in the radius of 500 m from the landslide are considered to count the human population.

Table 2 Details of the satellite imagery.

Satellite data		Source	Date of data	Spatial resolution
CARTOSAT-1 stereo imagery	524/253	National Remote Sensing Center (NRSC), Hyderabad, India	5thDec. 2010	~2.5 m
	525/253		16thDec. 2010	~2.5 m
	526/252		18thOct. 2011	~2.5 m
	526/253		18thOct. 2011	~2.5 m
	527/252		24thNov .2010	~2.5 m
	527/253		27thDec. 2010	~2.5 m
	528/252		26thNov. 2011	~2.5 m

Table 3 Criteria used in the Finite Element Method (FEM) analysis.

Material Criteria		**Parameters**	**Source**
Rockmass	**Generalized Hoek & Brown (GHB) Criteria** (Hoek et al. 1995) $\boldsymbol{\sigma_1 = \sigma_3 + \sigma_{ci}[m_b(\sigma_3/\sigma_{ci}) + s]\text{^}a}$ Here, σ_1 and $\sigma 3$ are major and minor effective principal stresses at failure; σ_{ci} , compressive strength of intact rock; m_b, a reduced value of the material constant (m_i) and is given by;	Unit Weight, γ (MN/m^3)	Laboratory analysis (UCS) (IS: 9143-1979)
		Uniaxial Compressive Strength, σ_{ci} (MPa)	
		Rockmass modulus (MPa)	Laboratory analysis (Ultrasonic velocity test); Hoek and Diederichs (2006).
		Poisson's Ratio	

	$m_b = m_i e^{[(GSI-100)/(28-14D]}$ s and a; constants for the rock mass given by the following relationships; $s = e^{[(GSI-100)/(9-3D]}$ $a = \frac{1}{2} + \frac{1}{6}\left[e^{[-(\frac{GSI}{15})]} - e^{[-(\frac{20}{3})]}\right]$ Here, D; a factor which depends upon the degree of disturbance to which the rock mass has been subjected by blast damage and stress relaxation. GSI (Geological Strength Index); a rockmass characterization parameter.	Geological Strength Index	Field observation and based on recent amendments (Cai et al. 2007 and reference therein)
		Material Constant (m_i)	Standard values (Hoek and Brown 1997)
		m_b	GSI was field depenedent, m_i as per(Hoek and Brown 1997) and D is used between 0-1 in view of rockmass exposure and blasting.
		s	
		a	
		D	
Joint	**Barton-Bandis Criteria** (Barton and Choubey 1977; Barton and Bandis 1990) $\tau = \sigma_n \tan [\emptyset_r + JRC \log_{10} (JCS/ \sigma_n)]$ Here,τ is joint shear strength;σ_n , normal stress across joint; $\emptyset_r$, reduced friction angle;JRC, joint roughness coefficient; JCS, joint compressive strength. JRC is based on the chart of Barton and Choubey (1977); Jang et al. (2014).JCS was determined using following equation; $\log_{10}(JCS) = 0.00088 (R_L)(\gamma)+1.01$ Here, R_L isSchimdt Hammer Rebound value and γ is unit weight of rock. The JRC and JCS were used as JRC_n and JCS_n. following the scale corrections observed by Barton and Choubey (1977) and reference therein and proposed by Barton and Bandis (1982). $JRC_n = [JRC(L/L_o)^{-0.02(JRC)}]$ $JCS_n = [JCS(L/L_o)^{-0.03(JRC)}]$ Here, Land L_o are mean joint spacing in field and, respectively. L_o has been suggested to be 10 cm. **Joint stiffness criteria** (Barton 1972) $k_n = (E_i * E_m)/L*(E_i - E_m)$ Here, k_n; Normal stiffness, E_i; Intact rock modulus, E_m; Rockmass modulus L; Mean joint spacing. $E_m=(Ei)*[0.02+\{1-D/2\}/\{1+e^{(60+15*D-GSI)/11)}\}]$ Here, E_m is based on Hoek and Diederichs (2006) and reference therein	Normal Stiffness, k_n (MPa/m)	E_i is lab dependent.L and GSI were field depenedent. D is used between 0-1 in view of rockmass exposure and blasting.
		Shear Stiffness , k_s (MPa/m)	It is assumed as $k_n/10$. However, effect of denominator is aslo obtainedthrough parameteric study.
		Reduced friction angle, $\emptyset_r$	Standard values (Barton and Choubey 1977).
		Joint roughness coefficient, JRC	Field based data from profilometer and standard values from Barton and Choubey (1977); Jang et al. (2014).
		Joint compressive strength, JCS (MPa)	Empirical equationof Deere and Miller (1966) relating Schimdt Hammer Rebound (SHR) values, σ_{ci} and unit weight of rock. SHR was field dependent.
		Scale corrected, JRC_n	Empirical equation of Barton and Bandis (1982).
		Scale corrected, JCS_n (MPa)	
	Mohr-Coulomb Criteria	Unit Weight (MN/m^3)	Laboratory analysis (UCS) (IS: 2720-Part 4–1985; IS: 2720-Part 10-1991)

Soil	(Coulomb 1776; Mohr 1914) $\boldsymbol{\tau = C + \sigma\, tan\emptyset}$ Here, τ; Shear stress at failure, C; Cohesion, σ_n; normal strength, Ø; angle of friction.	Young's Modulus, E_i (MPa)	Laboratory analysis (UCS); IS: 2720-Part 10-1991.
		Poisson's Ratio	Standard values from Bowles (1996)
		Cohesion, C (MPa)	Laboratory analysis (Direct shear) (IS: 2720-Part 13- 1986)
		Friction angle, Ø	

Table 4 Details of input parameters for run-out analysis. S.N. refers to serial number of landslides in Fig. 1.

Landslide	**Material type**	**Material depth[1], m**	**Friction coefficient[2]**	**Turbulence coefficient[3], m/sec^2**
Akpa (S.N. 5)	Gravelly sand	5	μ= 0.05, 0.1, 0.3	ξ = 100, 200, 300
Baren Dogri (S.N. 7)	Gravelly sand	1.25	μ= 0.05, 0.1, 0.4	ξ = 100, 200, 300
Pawari (S.N. 14)	Gravelly sand	1.25	μ= 0.05, 0.1, 0.4	ξ = 100, 200, 300
Telangi (S.N. 15)	Gravelly sand	6.25	μ= 0.05, 0.1, 0.4	ξ = 100, 200, 300
Urni (S.N. 19)	Gravelly sand	2.5	μ= 0.06, 0.1, 0.4	ξ = 100, 200, 300

[1] Considering that fact that during the slope failure, irrespective of type of trigger, entire loose material might not slide down, the depth is taken as only ¼ (thickness) in the calculation.[2] Since the angle of run-out track (slope and river channel) varied a little beyond the suggested range 2.8º -21.8º or μ = 0.05-0.4 (Hungr et al., 1984; RAMMS v.1.7.0), we kept out input in this suggested range wherever possible to avoid the simulation uncertainty. [3]This range is used in view of the type of loose material i.e., granular in this study (RAMMS v.1.7.0).

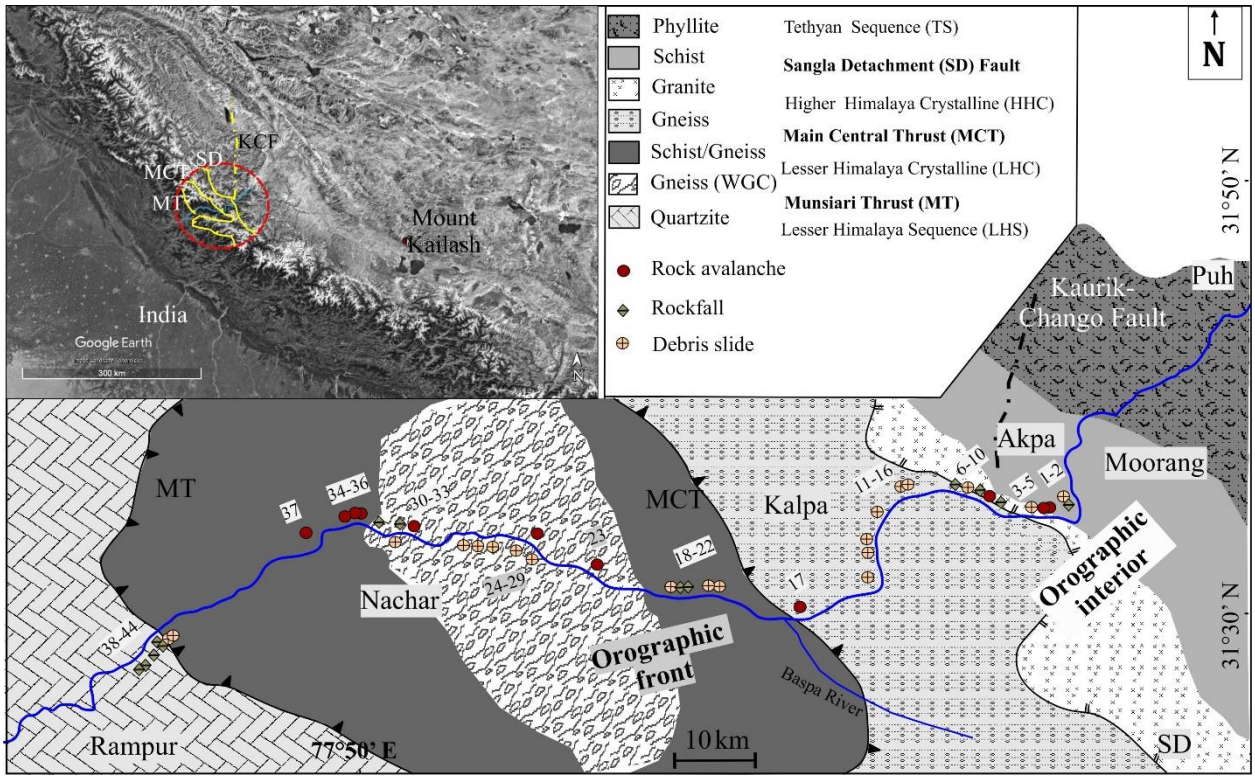

Fig. 1 Geological setting. WGC: Wangtu Gneissic Complex. The red dashed circle in the inset represents the region within 100 km radius from the Satluj River (marked as blue line) that was used to determine the earthquake distribution in the area. Yellow lines represent the regional faults in the region. KCF in inset refers to Kaurik-Chango Fault. The numbers 1-44 refer to serial number of landslides in Table 1.

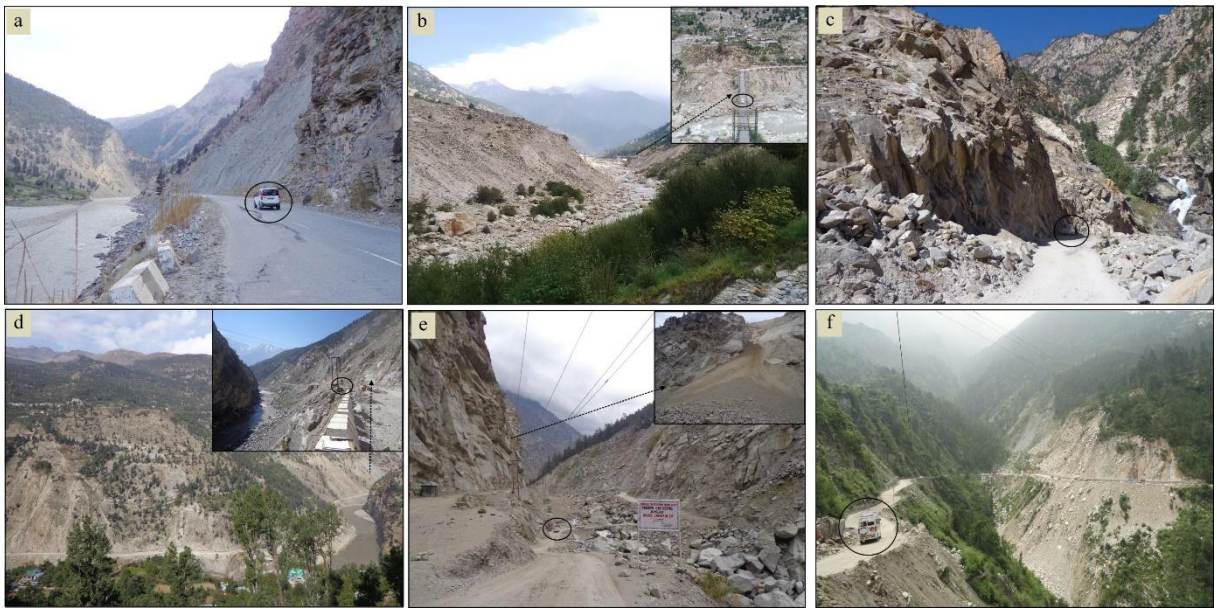

Fig. 2 Field photographs of some of the landslides (a) Khokpa landslide (**S.N.1**); (b) Akpa_III landslide (**S.N. 5**); (c) Rarang landslide (**S.N. 6**); (d) Pawari landslide (**S.N.14**); (e) Urni landslide (**S.N.19**); (f) Barauni Gad_I_S landslide (**S.N. 38**). Black circle in the pictures that encircles the vehicle is intended to represent the relative scale.

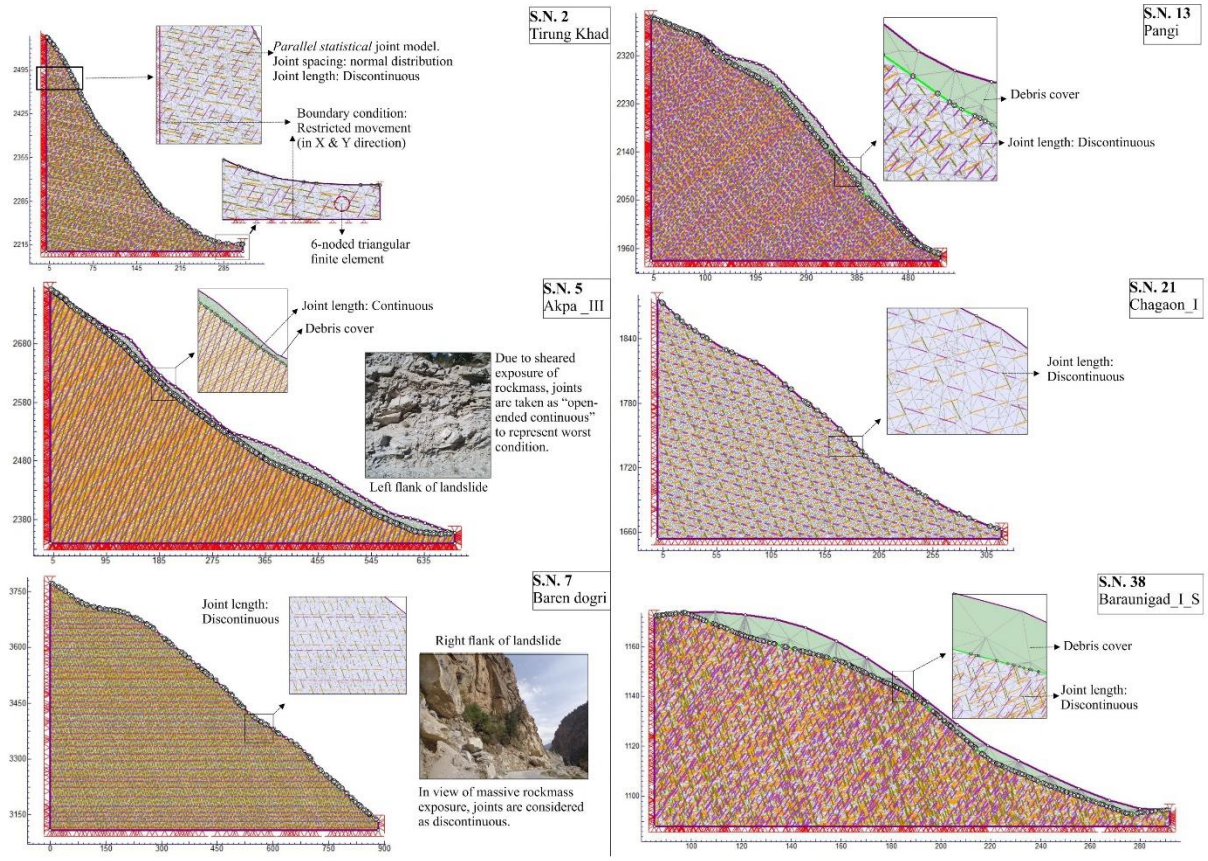

Fig. 3 The FEM configuration of some of the slope models. S.N. refers to the serial no. of landslides in Table 1. The joint distribution in all the slopes was parallel-statistical with the normal distribution of joint spacing.

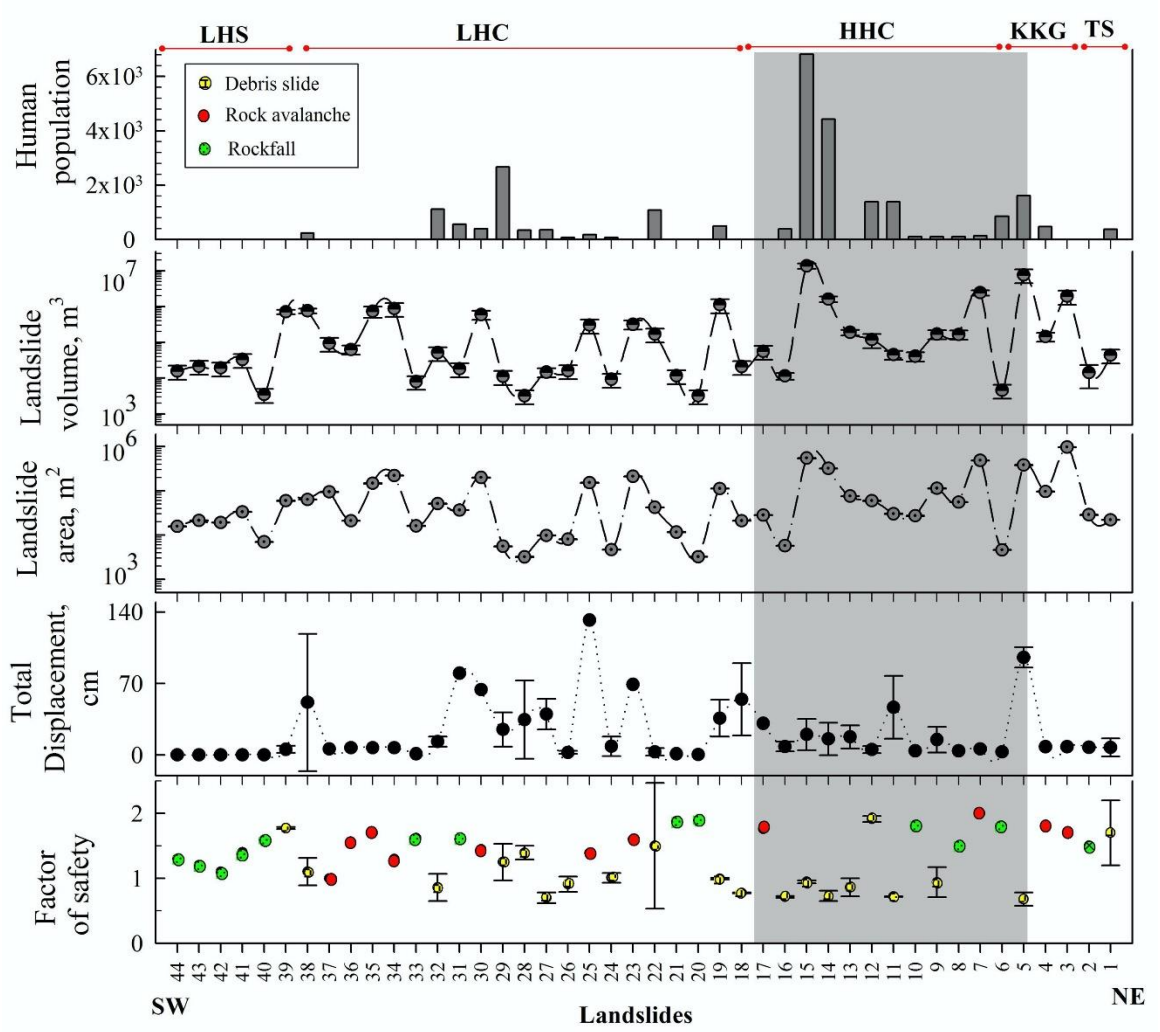

Fig. 4 The FEM analysis of all forty-four landslides. Grey bar in the background highlights the Higher Himalaya Crystalline (HHC) region that comprises relatively more unstable landslides, landslide volume and human population..TS, KKG, HHC, LHC and LHS are Tethyan Sequence, Kinnaur Kailash Granite, Higher Himalaya Crystalline, Lesser Himalaya Crystalline and Lesser Himalaya Sequence, respectively.

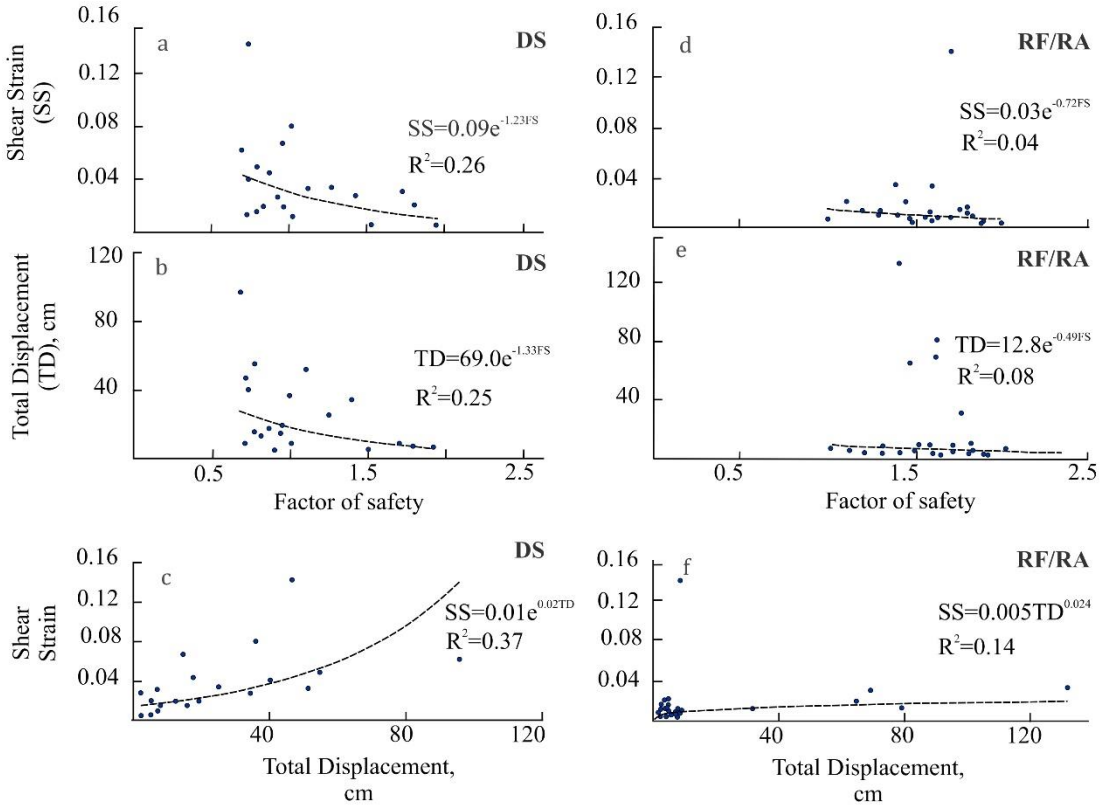

Fig. 5 Relationship of Factor of Safety (FS), Total Displacement (TD) and Shear Strain (SS). DS, RF, and RA refer to Debris slide, rock fall and rock avalanche, respectively.

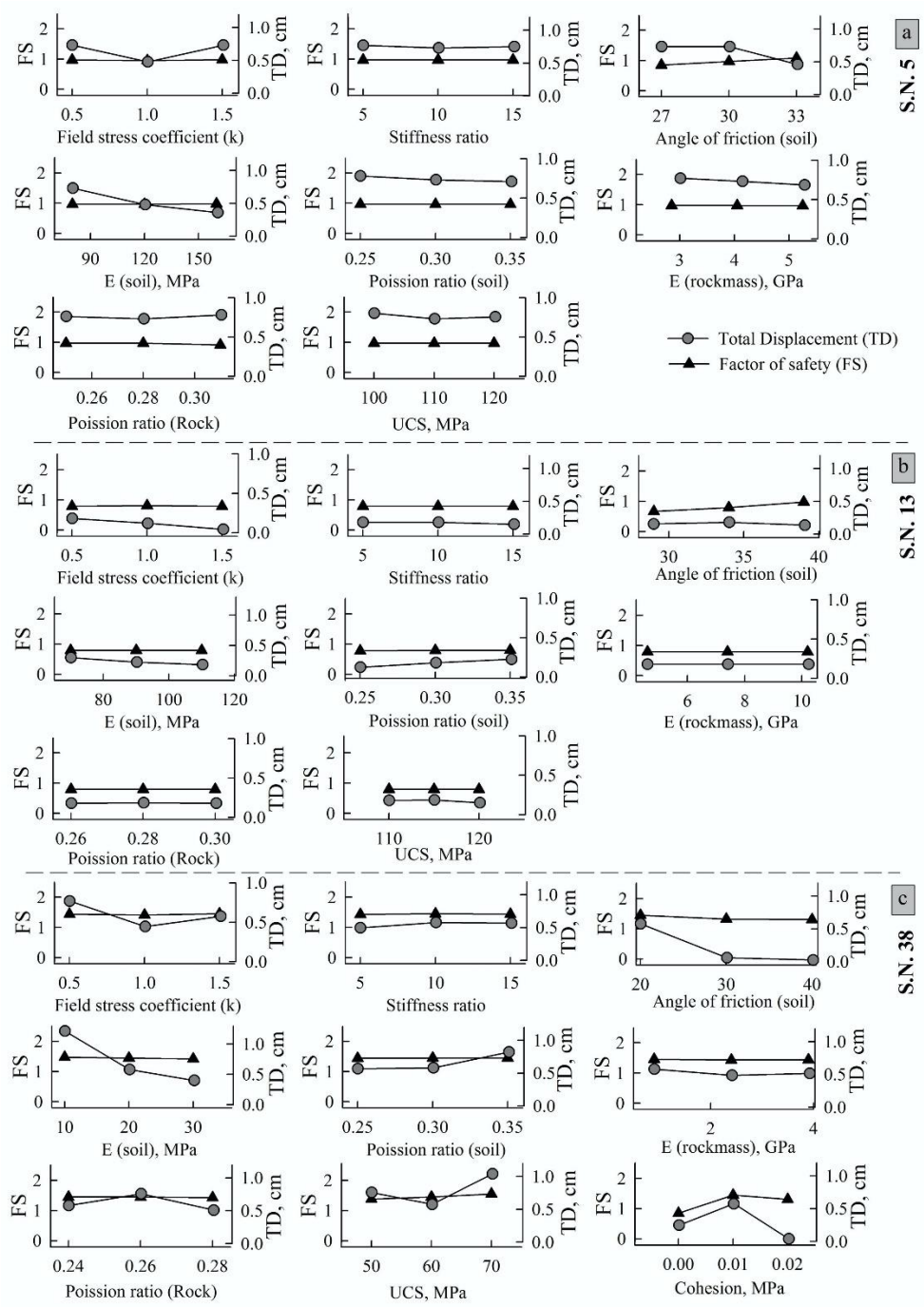

Fig. 6 Parametric analysis of debris slides. (a) Akpa_III (S.N. 5); (b) Pangi_III (S.N. 13); (c) Barauni Gad_I_S (S.N. 38). S. N. refers to the serial no. of landslides in Table 1.

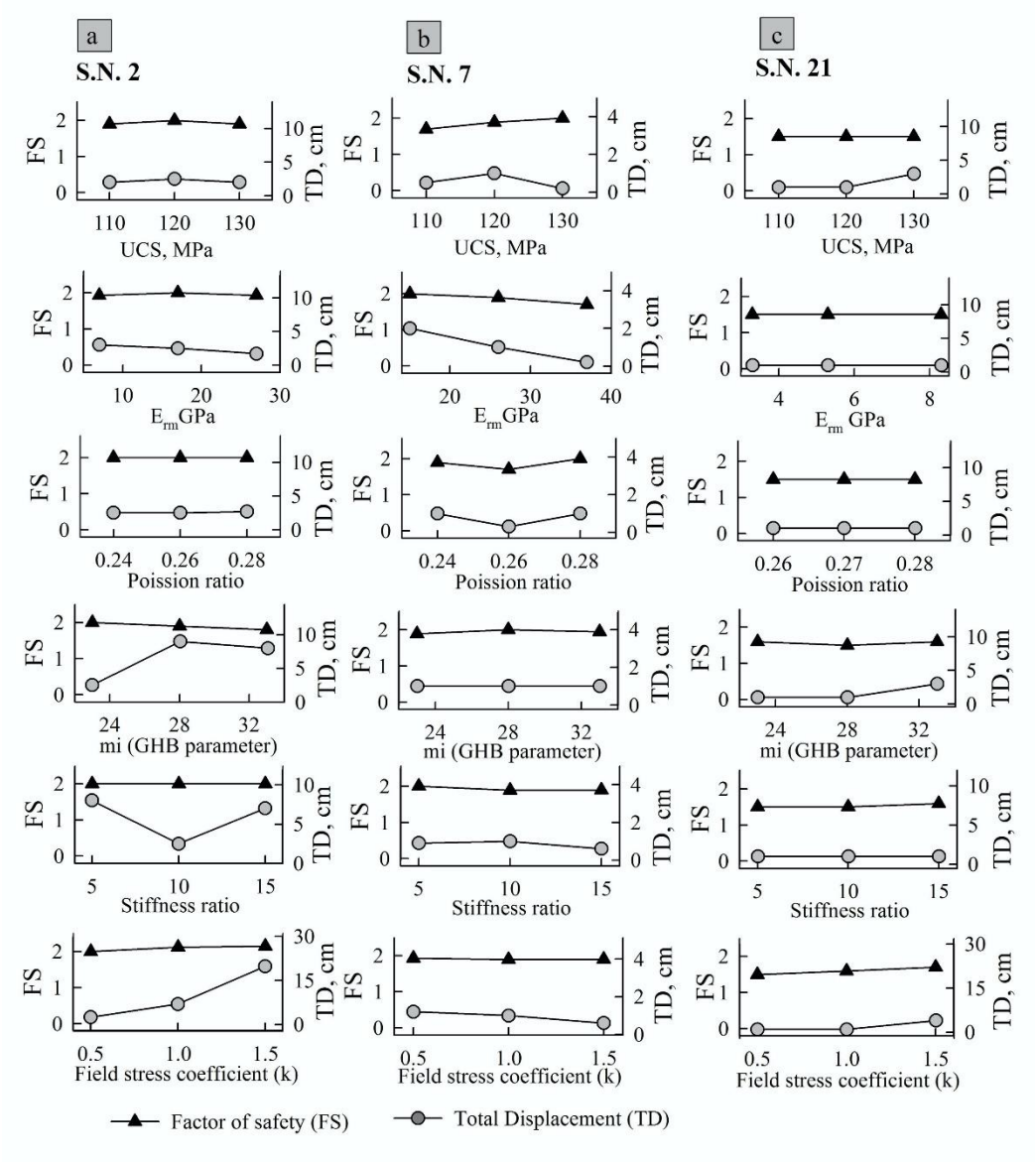

Fig. 7 Parametric analysis of rockfall/rock avalanche. (a) Tirung khad (S.N. 2); (b) Baren Dogri (S.No. 7); (c) Chagaon_II (S.N. 21).

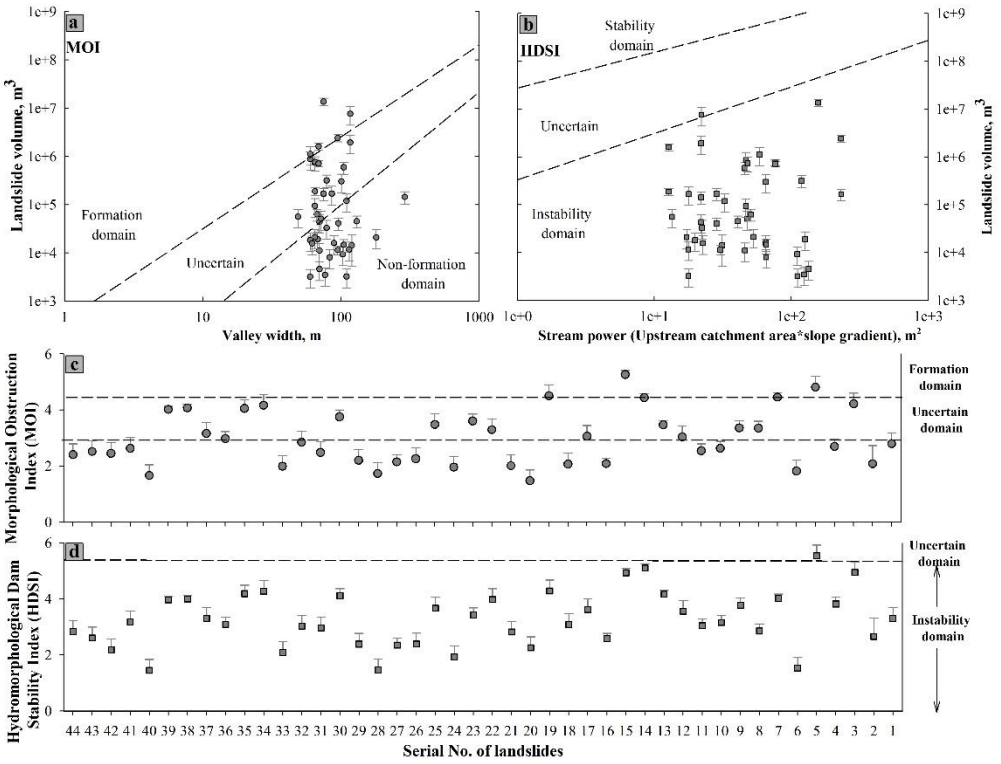

Fig. 8 Landslide damming indices (a) Morphological Obstruction Index (MOI); (b) Hydro-morphological dam stability index (HDSI); (c) Landslides vs. MOI; (d) Landslides vs. HDSI.

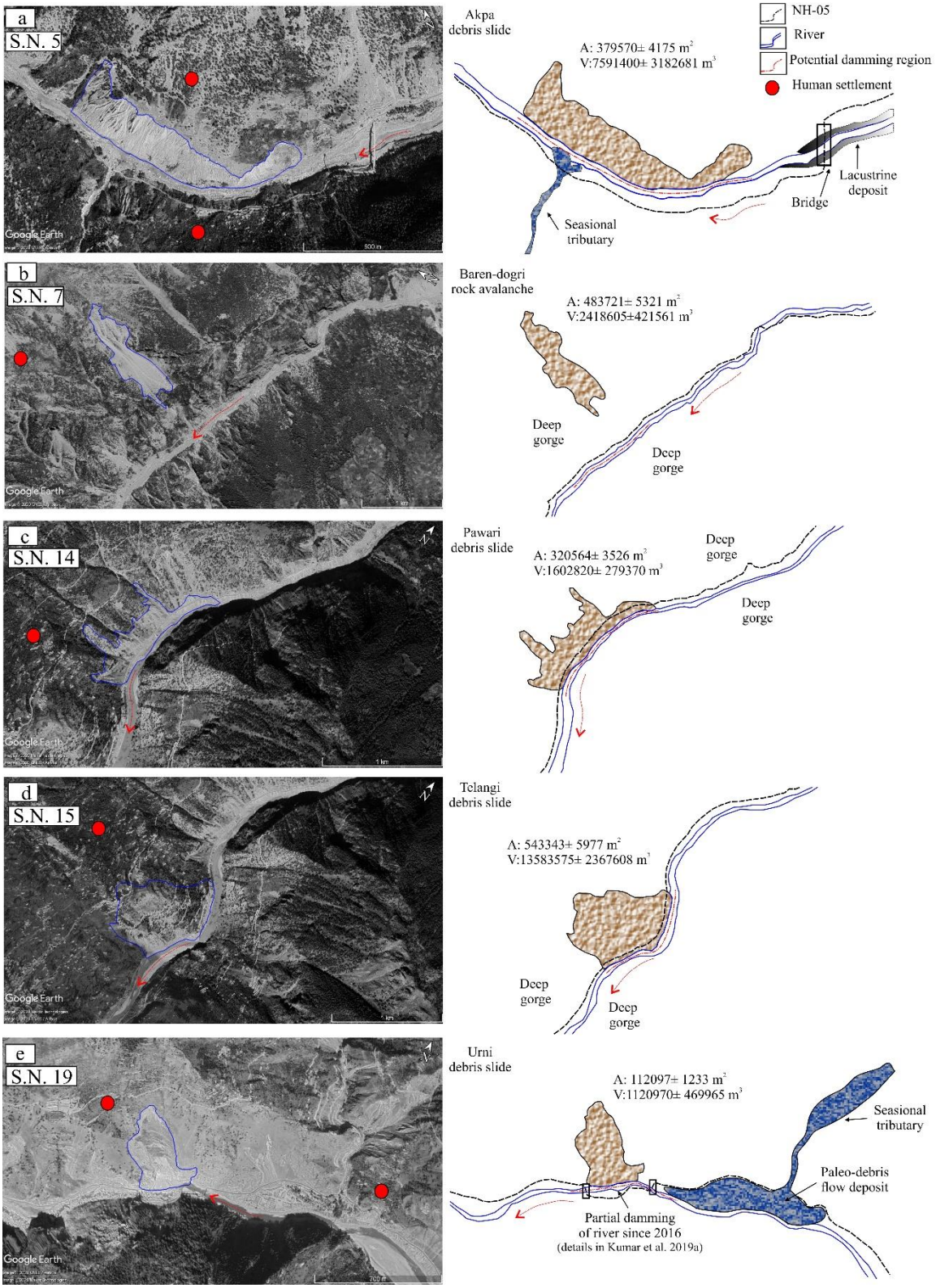

Fig. 9 Potential landslide damming locations. (a) Akpa_III landslide; (b) Baren dogri landslide; (c) Pawari landslide; (d) Telangi landslide; (e) Urni landslide. Red dashed-arrow represents the direction of river flow.

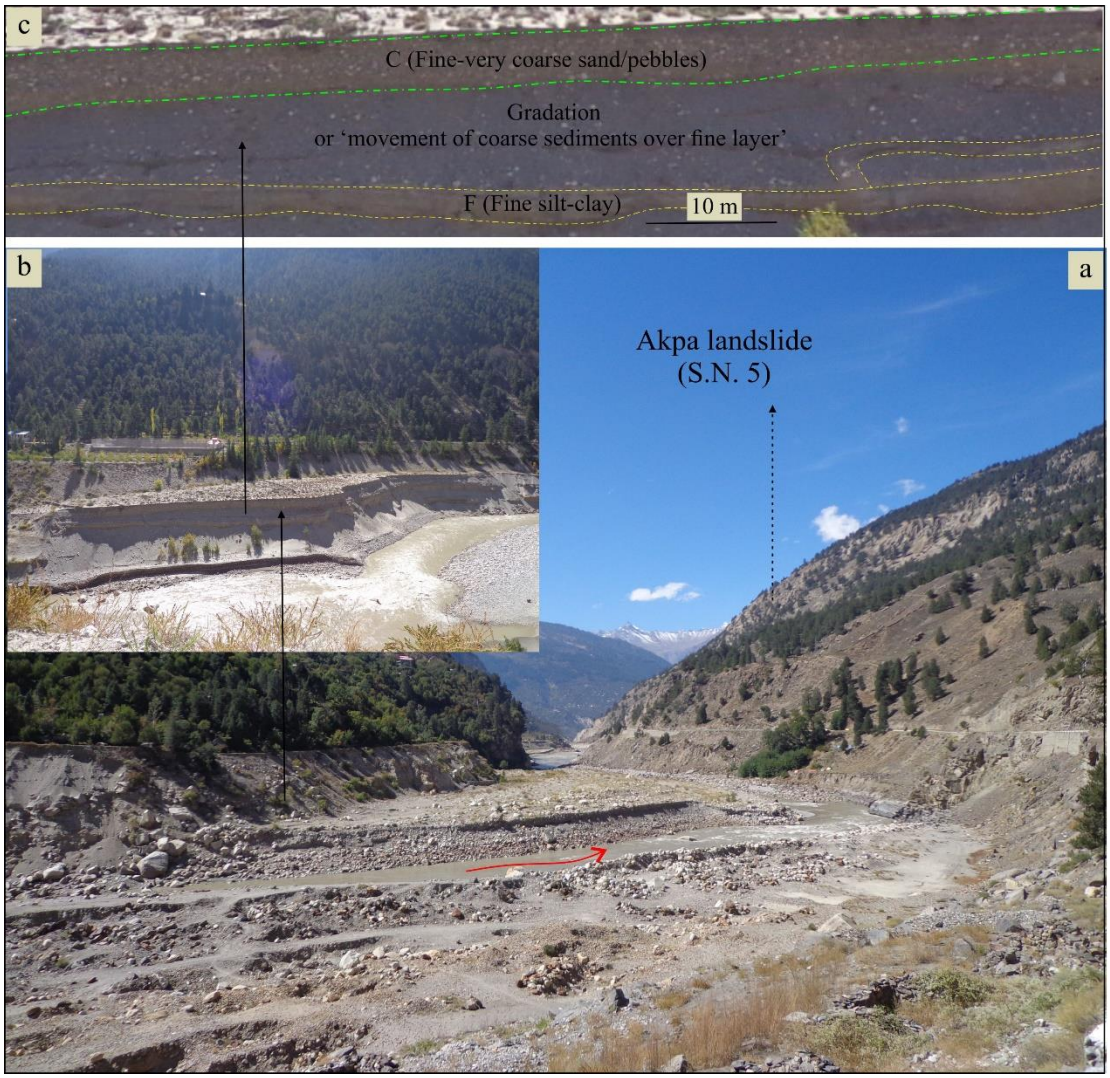

Fig. 10 Field signatures of the landslide damming near Akpa_III landslide. (a) Upstream view of Akpa landslide with lacustrine deposit at the left bank; (b) enlarged view of the lacustrine deposit with an arrow indicating the lacustrine sequence; (c) alternating fine-coarse sediments. F and C refer to fine (covered by yellow dashed lines) and coarse (covered by green dashed lines) sediments, respectively.

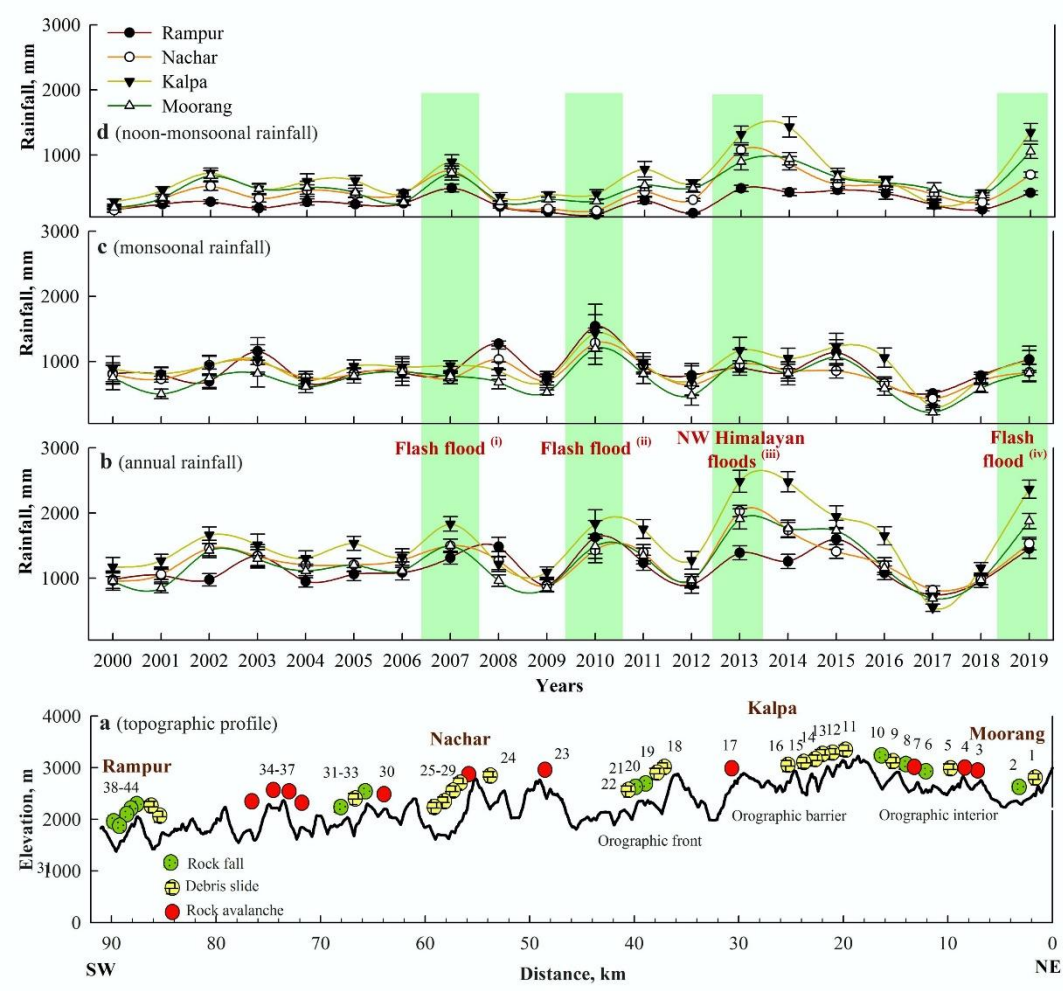

Fig. 11 Rainfall distribution. (a) Topographic profile; (b) annual rainfall; (c) monsoonal (June-Sep.) rainfall; (d) non-monsoonal (Oct.-May) rainfall. Green bars represent the years of relatively more rainfall resulting into the flash floods, landslides and socio-economic loss in the region. (i):hpenvis.nic.in, retrieved on March 1, 2020; Department of Revenue, Govt. of H.P. (ii): hpenvis.nic.in, retrieved on March 1, 2020.(iii): Kumar et al., 2019a;ndma.gov.in, retrieved on march 1, 2020 (iv):sandrp.in, retrieved on march 1, 2020.The numbers 1-44 refer to serial number of the landslides.

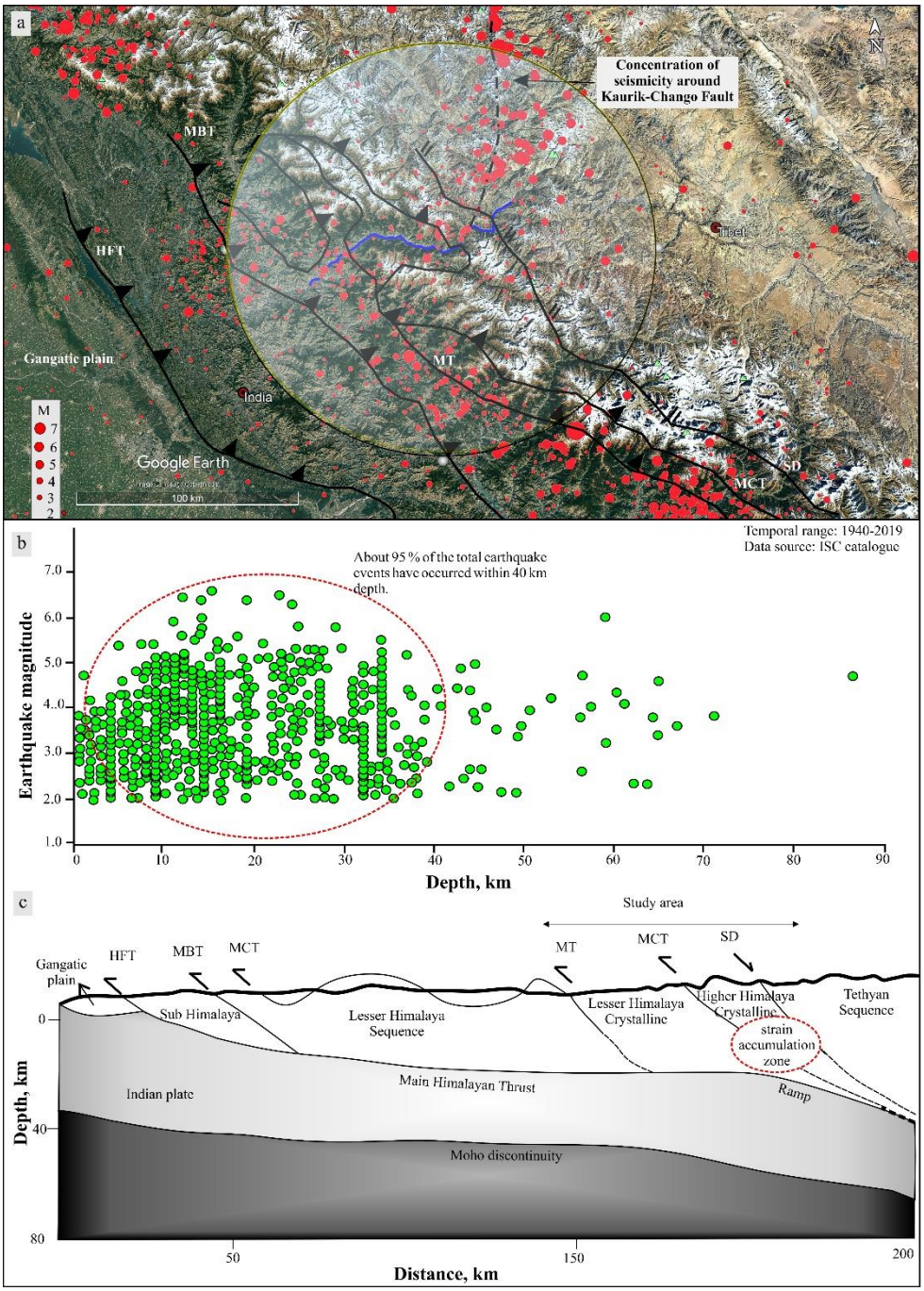

Fig. 12 Earthquake distribution. (a) Spatial variation of earthquakes. The transparent circle represents the region within 100 km radius from the Satluj River (blue line). The black dashed line represents the seismic dominance around the Kaurik-Chango fault;(b) earthquake magnitude vs. focal depth. The red dashed region highlights the concentration of earthquakes within 40 km depth; (c) Cross section view (Based on Hazarika et al. 2017; Bilham, 2019). Red dashed circle represents the zone of strain accumulation caused by the Indian and Eurasian plate collision (Bilham, 2019). ISC: International Seismological Centre. HFT: Himalayan Frontal Thrust.

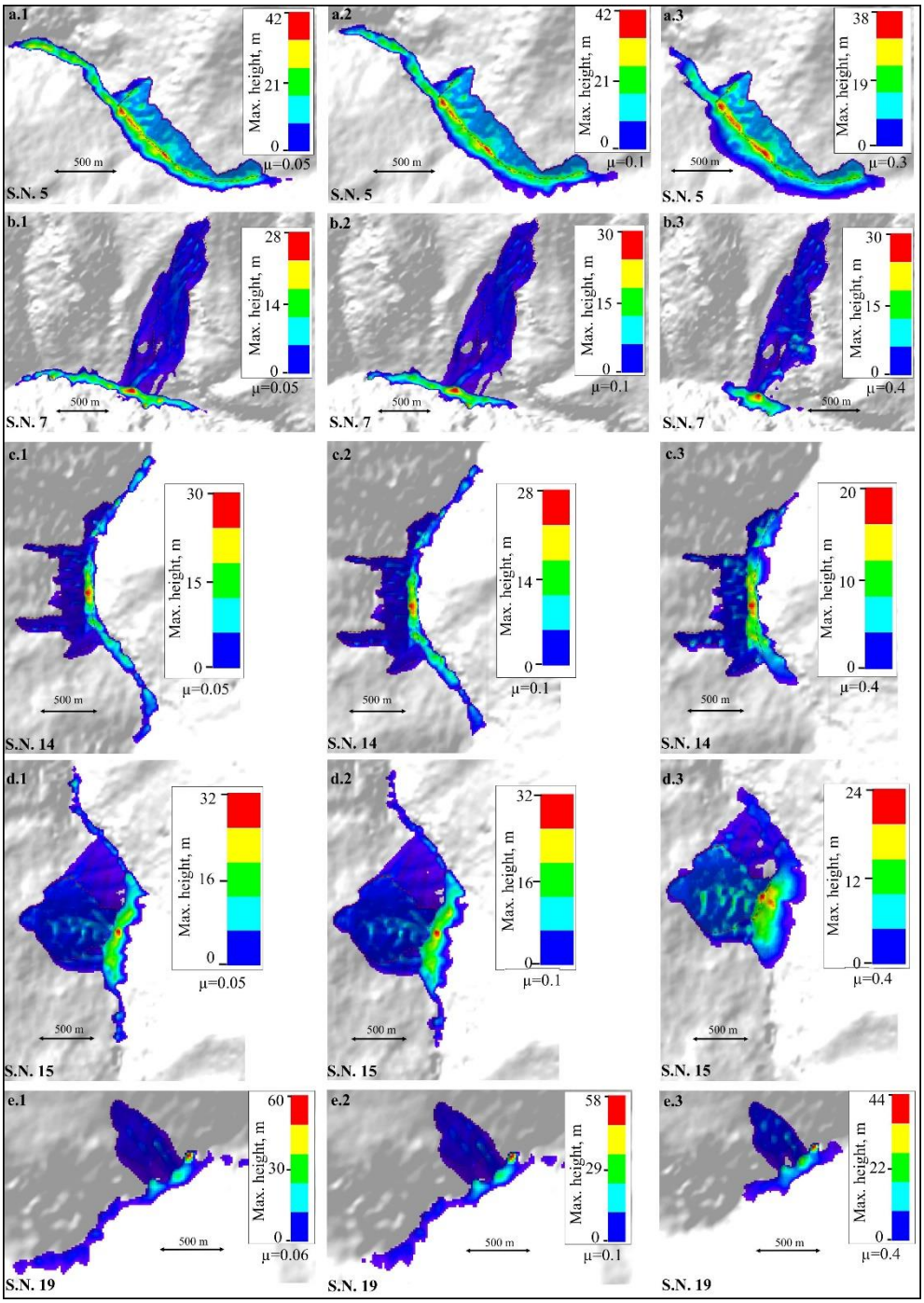

Fig. 13 Results of the run-out analysis. μ refers to coefficient of friction.

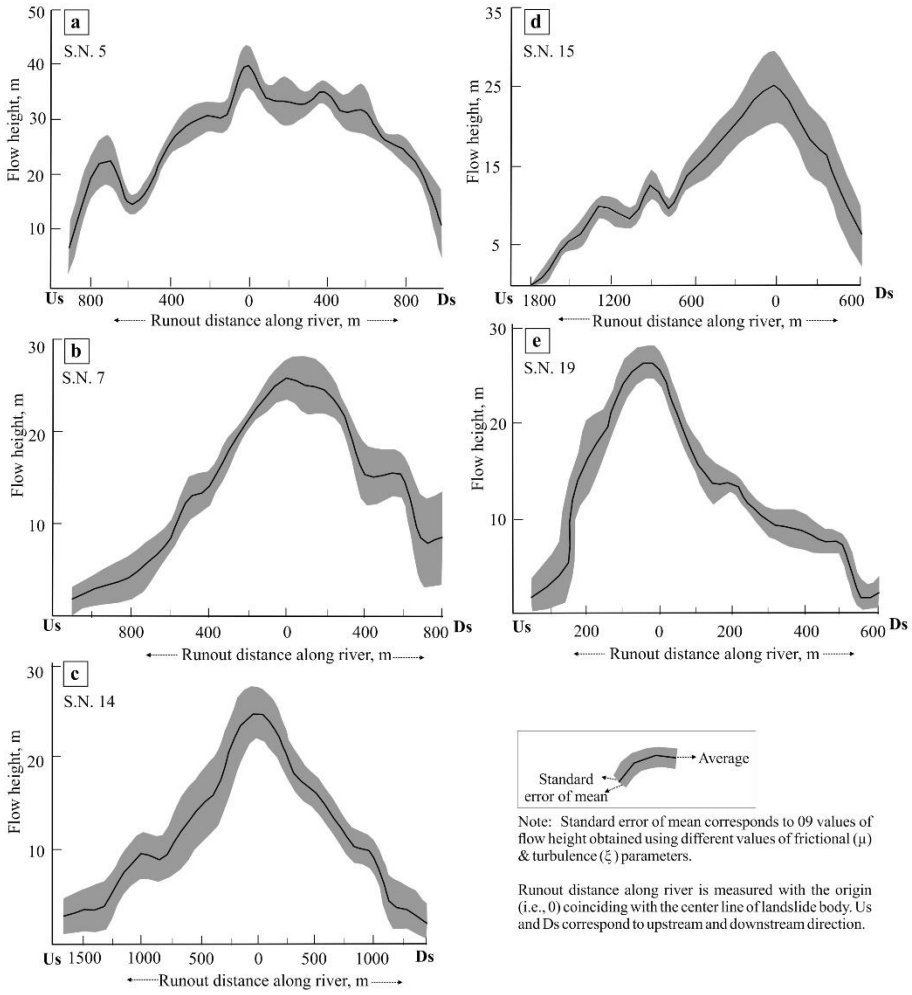

Fig. 14 Results of run-out analysis at different values of μ and ξ. μ and ξ refer to coefficient of friction and turbulence, respectively.